



Geochronology and geochemistry of Late Cretaceous igneous intrusions and Mo–Cu–(W) mineralization in the southern Yidun Arc, SW China: Implications for metallogenesis and geodynamic setting

Xin-Song Wang ^{a,b}, Xian-Wu Bi ^{a,*}, Cheng-Biao Leng ^a, Hong Zhong ^a, Hong-Feng Tang ^a, You-Wei Chen ^a, Guang-Hou Yin ^c, Ding-Zhu Huang ^c, Mei-Fu Zhou ^d

^a State Key Laboratory of Ore Deposits Geochemistry, Institute of Geochemistry, Chinese Academy of Sciences, Guiyang 550005, China

^b University of Chinese Academy of Sciences, Beijing 100049, China

^c Yunnan Bureau of Geological Survey, Kunming 650051, China

^d Department of Earth Sciences, The University of Hong Kong, Hong Kong 999007, China



ARTICLE INFO

Article history:

Received 1 July 2013

Received in revised form 11 January 2014

Accepted 20 January 2014

Available online 28 January 2014

Keywords:

Zircon U–Pb

Molybdenite Re–Os

Porphyry Mo–Cu deposits

Meso-Tethys

Yidun Arc

Sanjiang

ABSTRACT

The Sanjiang Tethyan Metallogenic Domain (STMD) is an important part of the Tethyan giant metallogenic belt. The Yidun Arc is a part of the STMD in the eastern Tibetan Plateau. Recently, four newly discovered Mo–Cu–(W) ore deposits related to granitic intrusions were found distributed along the north-south strike in the southern Yidun Arc, which are identified as the Xiuwacu, Relin, Hongshan, and Tongchanggou deposits herein. These four deposits formed along high-angle north-northwest or north-west strike-slip faults, with vein-type and porphyry-type Mo–Cu mineralization developed in the intrusions. Molybdenite Re–Os and zircon U–Pb dating together with zircon Hf isotopes and whole-rock geochemistry of the intrusions were studied to discern the relationship between mineralization and magmatism, metallogenesis, and tectonic settings. Molybdenite from skarn-type mineralization at the Hongshan deposit has a Re–Os isochron age of 81.2 ± 2.6 Ma (MSWD = 1.3, n = 5) consistent with previously published zircon U–Pb ages and Re–Os ages of porphyry-type Mo mineralization. These results indicate that the Hongshan is a Late Cretaceous porphyry-skarn Cu–Mo deposit. Zircon U–Pb ages of the granitic intrusions in the Xiuwacu, Relin, and Tongchanggou deposits varying from ~87.4 Ma to ~82.7 Ma. Combined with published molybdenite Re–Os age spectrum (~85 Ma to ~81.2 Ma), it is proposed that the Mo–Cu–(W) mineralization in the Shangri-La region is spatially, temporally, and probably genetically related to the Late Cretaceous granitic intrusions. The Relin, Hongshan, and Tongchanggou intrusions have high SiO₂ (65.2–70.0 wt.%), Sr (363–905 ppm), Sr/Y (22–72), and La/Yb (37–69) ratios, and low Y (11.6–17.0 ppm) and Yb (0.97–1.59 ppm), which displayed adakitic affinities. Their low MgO (0.66–1.44 wt.%), Mg# (25–46), variable negative zircon $\epsilon_{\text{Hf}}(\text{t})$ values (−7.9 to −2.3), and Proterozoic two-stages Hf model ages ($T_{\text{DM2}} = 1.13$ –1.62 Ga) suggest that they were probably dominantly derived from partial melting of thickened lower continental crust. According to the tectonic evolution of the Bangong Meso-Tethys Ocean during the Late Mesozoic, the Late Cretaceous igneous event and mineralization in the Yidun Arc likely formed under a late- or post-collision extensional environment, probably related to the collision between the Lhasa and Qiangtang terranes during the Late Cretaceous.

© 2014 Elsevier B.V. All rights reserved.

1. Introduction

The Sanjiang Tethyan Metallogenic Domain (STMD) is a significant part of the Tethyan giant metallogenic belt in the eastern Tibetan Plateau (Fig. 1a; Hou et al., 2007; Zaw et al., 2007) and has a complex history that involved ocean-continent subduction and continent-continent collision (Metcalfe, 2006, 2013; Mo et al., 2001; Pan et al., 2012). Porphyry Cu ± Mo ± Au mineralization events in

the STMD occurred in the Indosinian (250–200 Ma) and Himalayan periods (<65 Ma), and extensive documentation relates these events to the closure of the Paleo-Tethys Ocean and the subsequent India-Asia continental collision, respectively (Deng et al., 2010, 2012; Hou et al., 2003b, 2007; Pan et al., 2003). Yanshanian (200–65 Ma) porphyry Mo ± Cu mineralization in the STMD is known in the literature, but it remains poorly studied (Hou et al., 2007; Pan et al., 2003).

The Yidun Arc is a Late Triassic continental arc in the STMD located on the east side of the Qiangtang Terrane (Hou et al., 2003b). Recently, four Late Cretaceous Mo–Cu deposits (molybdenite Re–Os ages ranging from 83 Ma to 77 Ma; Xu et al., 2006; Li et al., 2007a, 2011a, 2012) have been reported in the Shangri-La region of the southern Yidun Arc (also

* Corresponding author. Tel.: +86 851 589 1962; fax: +86 851 589 1664.

E-mail addresses: gxygsw@hotmail.com (X.-S. Wang), bixianwu@vip.gyig.ac.cn (X.-W. Bi).

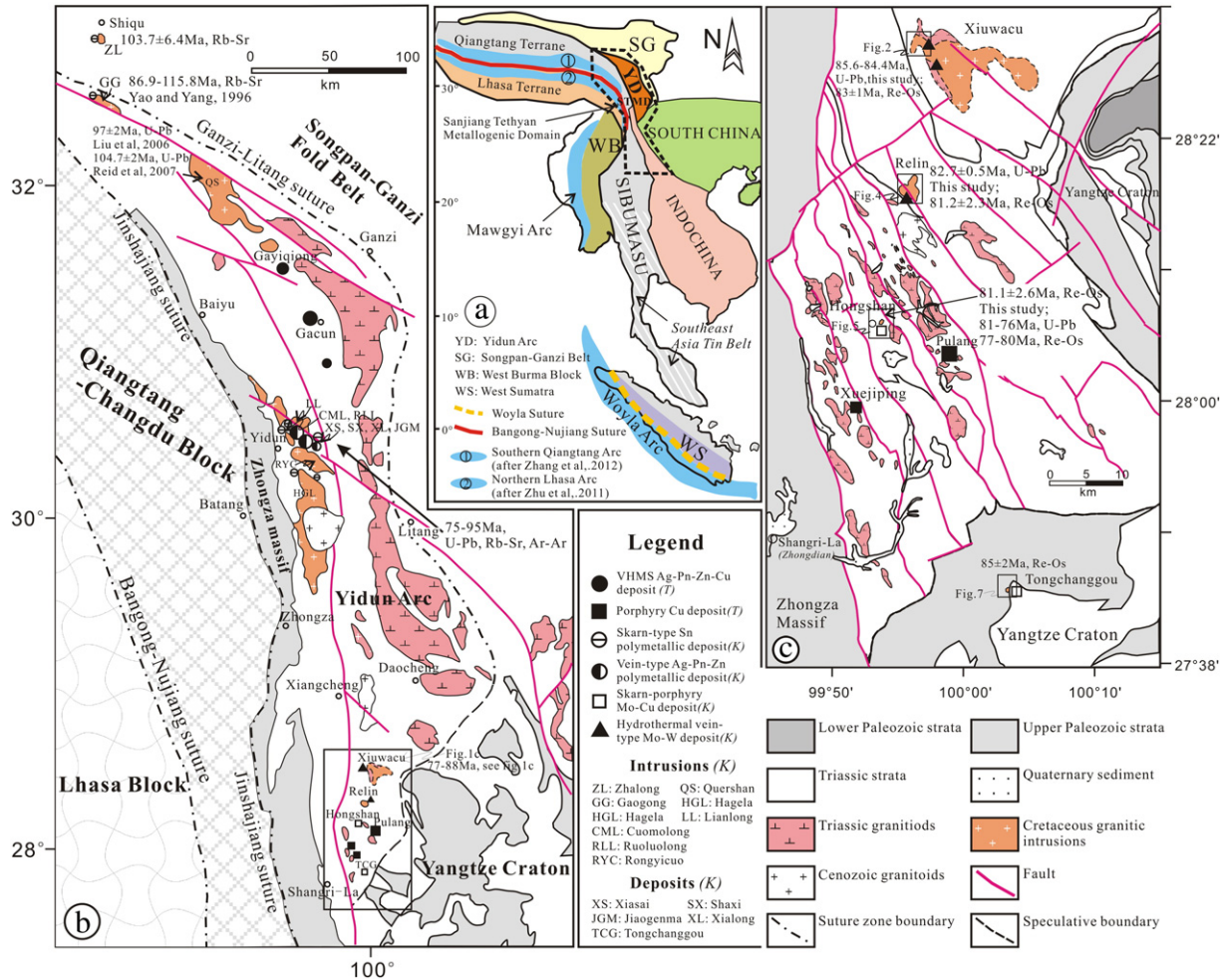


Fig. 1. (a) Regional location map showing terranes accreted in the Late Palaeozoic, in part based on previous studies (Metcalfe, 2011; Morley, 2012; Schwartz et al., 1995; Zhang et al., 2012; Zhu et al., 2011a), and simplified geological maps of (b) the Yidun Arc (modified after Hou et al., 2007) and (c) the Shangri-La region (modified after unpublished geological map from Yunnan Bureau of Geological Survey). (a) Illustration shows the Jurassic–Early Cretaceous arc-related magmatic belt in the southern Qiangtang Terrane and northern Lhasa Terrane, and the position and scope of the Sanjiang Tethyan Metallogenic Domain (STMD), Southeast Asian Tin Belt, Mawgyi Terrane, and Woya Terrane; (b) and (c) show the distribution of the Triassic (*T*) and Cretaceous (*K*) deposits and associated intrusions in the Yidun Arc and the Shangri-La region, respectively. References to the ages of mineralization and intrusions in Zhalong, Xiasai, Shaxi, Lianlong, Cuomolong, Xiuwacu, Relin, Hongshan, and Tongchanggou are listed in Table 1.

known as the Zhongdian Arc). These newly reported Late Cretaceous deposits include the Xiuwacu Mo–W, Relin Mo–W–Cu, Hongshan Cu–, and Tongchanggou Mo–Cu deposits. They are spatially associated with granitic intrusions. However, the timing of igneous events and mineralization of these deposits are still poorly constrained. Available age data for the intrusions range from ~216 Ma to ~77 Ma (Huang et al., 2012; Wang et al., 2011b; Xu et al., 2006; Yang et al., 2002; Yin et al., 2009), which makes it difficult to understand their relationship to ore-forming processes. Moreover, because of the lack of geochemical data, it is difficult to understand their genesis and geodynamic settings. In addition, Cretaceous magmatism and mineralization also occur widely in the Lhasa Terrane, West Yunnan, and Southeast Asian Tin Belt (Morley, 2012; Schwartz et al., 1995; Xu et al., 2012c; Zhang et al., 2012; Zhu et al., 2011a, 2013). The possibility that mineralization in the Yidun Arc may have been generated under similar geodynamic settings as these other examples has not been evaluated.

In this study, we present new zircon U–Pb dates obtained via laser ablation inductively coupled plasma mass spectrometry (LA-ICP-MS) for granites within the Xiuwacu, Relin, and Tongchanggou deposits and molybdenite Re–Os ages for the Hongshan polymetallic Cu–Mo deposit. With these dates and in conjunction with zircon Lu–Hf isotopes and whole-rock geochemical data we attempt (1) to

constrain the genetic link between the granitic intrusions and associated mineralization, (2) to discuss the tectonic settings of these Late Cretaceous deposits in the Yidun Arc, and (3) to unravel metallogenesis of the Late Cretaceous Mo–Cu mineralization in the southern Yidun Arc.

2. Regional geology

The Yidun Arc lies among the Qiangtang Terrane (west), Songpan-Ganzi Fold Belt (northeast), and Yangtze Craton (southeast), and it is bounded by the Jinshajiang Suture to the west and the Ganzi-Litang Suture to the east (Fig. 1a; Yang et al., 2012; Yin and Harrison, 2000). Both the Jinshajiang Ocean and the Ganzi-Litang Ocean are considered to be branches of the Paleo-Tethys (Metcalfe, 2006; Wang et al., 2000). The Bangong Suture, the northern branch of the Meso-Tethys between the Qiangtang and Lhasa terranes, is also located on the southwest side of the Yidun Arc (Fig. 1a, b; Metcalfe, 2011; Pan et al., 2012). The subduction polarity of the Bangong Meso-Tethys is debatable. It is generally considered that the subduction was northward with the widely distributed Jurassic and Cretaceous arc magmatism on the southern Qiangtang Terrane (Zhang et al., 2012 and references therein). Whereas, in consideration of the presence of calc-alkaline andesites with ages of

131–115 Ma and the trend for decreasing zircon $\epsilon_{\text{Hf}}(t)$ values from the northern to the central Lhasa Terrane, Zhu et al. (2009a, 2011a) suggested that the Bangong Meso-Tethys seafloor was subducted southwards beneath the Lhasa Terrane. This south-dipping model is further supported by recently obtained geological, geochronological, and geochemical data (Qu et al., 2012; Shi et al., 2004; Sui et al., 2013). Meanwhile, a bidirectional-subduction model was also proposed to explain the occurrence of Cretaceous arc-related magmas on both the Lhasa and Qiangtang terranes (Du et al., 2011). In general, it is widely accepted that the initial collision of the Bangong Meso-Tethys occurred during the Late Jurassic and Early Cretaceous (earlier in the east and later in the west) (Kapp et al., 2005, 2007). However, the Bangong Tethys was not closed until the Late Cretaceous (Zhang et al., 2012) following intense indentation of the Lhasa Terrane (Zhu et al., 2011a). In addition, many studies indicate that the southern segments of the Meso-Tethys (Mawgyi and Woya terranes; Fig. 1a) were also not finally closed and collision continued into the Late Cretaceous (Morley, 2012 and references therein).

The Yidun Arc is composed of the Zhongza Massif (the western Yidun Arc) and the eastern Yidun Arc (Fig. 1b; Hou and Mo, 1991; Hou et al., 2003b; Reid et al., 2005b). The Zhongza Massif consists of carbonate-dominated Palaeozoic metasedimentary rocks intercalated with mafic volcanic rocks (Chang, 1997). Some workers inferred that the Zhongza Massif is a “microcontinent,” which was separated from the Yangtze Craton in the Late Permian by the opening of the Ganzi-Litang Ocean. Palaeozoic metasedimentary rocks in the Zhongza Massif have fossil assemblages similar to those of the equivalent strata of the western Yangtze Craton (Chang, 1997; Hou et al., 2003b). The Triassic volcanic rocks in the eastern Yidun Arc show geochemical affinities with continental arc volcanic rocks (Hou and Mo, 1991; Hou and Zhou, 2001; Mo et al., 2001; Zhu et al., 2011b). The Triassic granitoids in the western Yidun Arc contain inherited zircons with ages correlated to the Yangtze Craton (Reid et al., 2007). The eastern Yidun Arc is composed of north-south tending Late Triassic volcanic-sedimentary successions with Late Triassic granitoids formed in response to the westward subduction of the Ganzi-Litang Ocean crust (Hou, 1993; Hou and Mo, 1991; Hou et al., 2003b). However, there were distinct mineralization styles between the northern and southern sections of the eastern Yidun Arc during the Late Triassic and Cretaceous. In the north, there are not only Late Triassic bimodal volcanic suites and related VHMS deposits, including Gacun and Gayiqiong Ag-Pb-Zn polymetallic VHMS deposits (Fig. 1b; Hou and Mo, 1991; Hou et al., 2001a, 2003b, 2007; Wang et al., 2013), but also Cretaceous intrusions and related skarn-type Sn-Ag polymetallic deposits and hydrothermal vein-type Ag-Pb-Zn polymetallic deposits commonly found in the Baiyu-Batang region (Fig. 1b; Hou et al., 2007; Lin, 2010; Lin et al., 2003; Liu, 2003; Qu et al., 2001). These deposits form an important Sn-Ag-Pb-Zn polymetallic sub-belt with more than 17,000 t of Ag, 0.27 Mt of Sn, and 4.79 Mt of Pb + Zn (Table 1). Many studies suggest that these Cretaceous intrusions are A-type granites ranging in ages from 115 Ma to 75 Ma, and probably formed in an intra-continental extension setting by lithosphere delamination after the collision between the Songpan-Ganzi Belt and Yidun Arc (Fig. 1b; Table 1; Fan, 2009; Guan, 1999; Hou et al., 2003b; Liao and Yao, 1995; Lin, 2010; Lin et al., 2003; Liu, 2003; Liu et al., 2006; Qu et al., 2001, 2002; Reid et al., 2005a, 2007; Ying et al., 2006; Zhang, 1994; Zou et al., 2008).

The southern portion of the eastern Yidun Arc (i.e., the Shangri-La region) is composed mainly of Late Triassic volcanic-sedimentary successions intruded by contemporaneous intermediate-felsic porphyries associated with porphyry-type or skarn-type Cu-polymetallic mineralization, including the Pulang and Xuejiping porphyry Cu-polymetallic deposits and Langdu skarn-type Cu-polymetallic deposit (Fig. 1b; Hou et al., 2003b; Zeng et al., 2003, 2004). These Late Triassic porphyritic intrusions are high-K calc-alkaline adakitic magmas with relative high $\epsilon_{\text{Nd}}(t)$ (−3.8 to −2.1) and $\epsilon_{\text{Hf}}(t)$ (−3.5 to 3.2) and with ages ranging from 206 Ma to 230 Ma (Leng et al., 2012; Liu and Li, 2013; Wang

et al., 2011a). They were proposed to be generated by partial melting of the metasomatized mantle with minor crustal contamination during the subduction of the Ganzi-Litang oceanic crust (Leng et al., 2012; Li et al., 2011b). In addition, there are four Mo-Cu deposits related to Late Cretaceous granitic intrusions in the region (Fig. 1b; Huang et al., 2012; Li et al., 2007a, 2011a, 2012; Wang et al., 2011b; Xu et al., 2006, 2012b; Yin et al., 2009).

3. Ore deposit geology

In the Shangri-La region, the four Cretaceous deposits are distributed along the north-south trend and consist of quartz-vein-type, skarn-type, and porphyry-type Mo-W or Cu-Mo mineralization. The ore bodies are all spatially associated with the granitic intrusions and controlled by high-angle north-northwest or north-west strike-slip faults (Fig. 1b).

3.1. Xiuwacu Mo-W deposit

This deposit is of a hydrothermal quartz-vein-type and is located ~80 km from Shangri-La (Zhongdian) City (Fig. 1c). The deposit contains a resource of 13,627 t Mo and 8431 t WO₃, with an average ore grade of 0.34% Mo and 0.28% WO₃ (Table 1). This deposit is divided into four ore blocks: North, East, West, and Sangdugele (Fig. 2a). Three stages of granitic intrusions are recognized in this deposit; these include the Late Triassic medium-coarse grained hornblende biotite monzogranite, Cretaceous medium-coarse grained biotite monzogranite, and medium-fine grained alkali-feldspar leucogranite. The sedimentary rocks in this district consist mainly of Late Triassic medium- to thick-bedded sandstone and slate. The ore bodies are hosted in hornblende biotite monzogranite and biotite monzogranite. Hydrothermal alteration consists mainly of K-feldspathization, greisenization, silification, argillization, and pyritization. The medium-fine grained alkali-feldspar leucogranite and associated disseminated scheelite and molybdenite mineralization are exposed in the North ore block. Furthermore, large quartz veins (20–100 m wide), K-Na feldspar, and fluorite megacrysts (3–20 cm) can be found at depth within the North ore block. The other three ore blocks are composed predominately of quartz-vein-type, greisens-type, and altered granite-type near the quartz vein. The ore bodies are distributed extending northwest along regional faults. Ore minerals include molybdenite, scheelite, bismuthinite, tennantite, chalcopyrite, pyrite, pyrrhotite, sphalerite, galena, and wolframite. Molybdenite is usually present as euhedral megacrysts (1–8 cm) that occur as fan-shaped sheets or stellate aggregates along the fracture surface of the intrusions. Scheelite occurs as allotriomorphic grains, light brown to light green in colour. Gangue minerals include quartz, K-feldspar, biotite, fluorite, and calcite.

3.2. Relin W-Mo-Cu deposit

The Relin hydrothermal quartz-vein-type W-Mo-Cu deposit is located ~55 km northeast (NE) from Shangri-La City where there have been low-levels of exploration (Fig. 1c). Medium-fine to coarse grain biotite monzogranite covering an area of 6.9 km² is exposed in the Relin district (Fig. 2b). The hanging wall comprises Late Triassic medium- to thick-bedded sandstone, slate, and Late Cretaceous biotite monzogranite. The alteration include greisenization, pervasive silification, intense pyritization, and weak skarn alteration (Yin et al., 2009). The four main ore bodies extending northwest in this region are 50–200 m long and 0.8–10 m wide; the average grade of Mo is 0.049% (Table 1). The mineralization styles include quartz veins, greisens, and altered granite type near quartz veins. The ore minerals are molybdenite, scheelite, chalcopyrite, pyrite, and pyrrhotite.

Table 1
Geological features of major Late Cretaceous ore deposits in the Yidun Arc.

Deposit (long/lat)	Location	Genetic type	Metals	Tonnage and grade	Host rocks	Alteration	Ore minerals	Related intrusions	Ages	Reference
Xiuwacu (99°57'; 28°30')	Shangre-La, Yunnan	Hydrothermal quartz-vein-type	Mo-W	Mo: 13,627 t @ 0.38%, WO ₃ : 8431 t @ 0.28%	Upper Triassic sandstone and slate	K-feldspathization, greisenization, silicification, argillization, pyritization	Molybdenite, scheelite, bismuthinite, tennantite, chalcopyrite, pyrite, pyrrhotite	Xiuwacu monzogranite	Zircon U-Pb age of the monzogranite: 84.4 ± 1.4 Ma to 85.6 ± 0.5 Ma, Molybdenite Re-Os isochronal age: 83 ± 1 Ma	This study, Li et al. (2007a)
Relin (99°56'; 28°17')	Shangre-La, Yunnan	Hydrothermal quartz-vein-type	Mo-W-Cu	Mo@0.049%	Upper Triassic sandstone and slate	Greisenization, silicification, pyritization and low-skarnization	Molybdenite, scheelite, chalcopyrite, pyrite, pyrrhotite	Relin monzogranite	Zircon U-Pb age of the monzogranite: 82.7 ± 0.5 Ma, ⁴⁰ Ar/ ³⁹ Ar age of biotite from monzogranite: 81.7 ± 0.9 Ma to 82.0 ± 0.9 Ma, Molybdenite Re-Os isochronal age: 81.2 ± 2.3 Ma	This study, Li et al. (2007a); Yin et al. (2009)
Hongshan (99°53'; 28°07')	Shangre-La, Yunnan	Porphyry-skarn type	Cu-Mo- polymetallic	Cu: 0.65 Mt @ 1.23%, S: 4.95 Mt @ 3.77%, Ag: 323 t @ 15.4 g/t, Mo: 5769 t, In: 253 t, Co: 1858 t, Bi: 6622 t, WO ₃ : 7532 t, Pb and Zn: 25,262 t	Upper Triassic sandy-slate, limestone, marble	Skarnization and marmorization	Pyrrhotite, chalcopyrite, pyrite, molybdenite, sphalerite	Hongshan granitic porphyry	Zircon U-Pb age of the granite porphyry in the deep: 75.8 ± 1.3 Ma, Zircon U-Pb age of the granite porphyry in the shallow: 81.1 ± 0.5 Ma, Molybdenite Re-Os isochronal age of the porphyry-type mineralization: 77 ± 2 Ma to 80.2 ± 1.3 Ma, Molybdenite Re-Os isochronal age of the skarn- type mineralization: 81.2 ± 2.6 Ma	This study, Xu et al. (2006), Li et al. (2007a), Li et al. (2011a), Wang et al. (2011b), Huang et al. (2012)
Tongchanggou (100°42'; 28°44')	Shangre-La, Yunnan	Porphyry-skarn type	Mo-Cu	Mo: 50,000 t @ 0.3%; Cu: 34,000 t @ 0.8%; Ag: 35 t @ 8.05 g/t;	Triassic limestone and marble, and Permian basalt	Skarnization and marmorization	Molybdenite, chalcopyrite, pyrite, magnetite	Dioritic porphyry	Zircon U-Pb age of diorite porphyry: 86.3 ± 0.6 Ma to 87.4 ± 0.6 Ma, Molybdenite Re-Os mean age: 85 ± 2 Ma	This study, Li et al. 2012.
Xiasai (99°36'; 30°27')	Batang, Sichuan	Hydrothermal vein-type	Ag-Pb-Zn- (Sn-Cu-Au)	Ag: 5600 t @ 300 g/ t, Pb: 0.73 Mt @ 8%, Zn: 0.44 Mt @ 2%, Sn: 20,000 t @ 0.19%	Upper Triassic sandstone, slate and little carbonatite	Pyritization, silicification, sericitization, chloritization, carbonatization	Galena, sphalerite, pyrite, chalcopyrite, native silver	Ruoluolong and Rongyicuo biotite monzogranite	⁴⁰ Ar/ ³⁹ Ar age of quartz from main mineralized vein in Xiasai deposit: 73.2 ± 0.3 Ma to 76.9 ± 0.6 Ma, ⁴⁰ Ar/ ³⁹ Ar plateau age of K-feldspar from Rongyicuo monzogranite: 75.2 ± 0.3 Ma, Rb-Sr isochronal ages of Rongyicuo monzogranite: 93 ± 5 Ma, Rb-Sr isochronal ages of Ruoluolong monzogranite: 93 ± 7 Ma	Zhang (1994), Liao and Yao (1995), Qu et al. (2001), Lin et al. (2003), Liu et al. (2006), Ying et al. (2006), Zou et al. (2008) Fan (2009), Lin (2010);

Shaxi (99°34', 30°26')	Batang, Sichuan	Hydrothermal vein-type	Ag–Pb–Zn–Sn–(Cu–Au–W)	Ag:>10,000 t, Pb and Zn:3Mt, Sn:0.10Mt	As above	As above	As above	As above	⁴⁰ Ar/ ³⁹ Ar plateau age of K-feldspar from Rongyicuo monzogranite: 75.2 ± 0.3 Ma, Rb–Sr isochronal ages of Rongyicuo monzogranite: 93 ± 5 Ma, Rb–Sr isochronal ages of Ruoluolong monzogranite: 93 ± 7 Ma	As above
Xialong (99°34', 30°24')	Batang, Sichuan	Hydrothermal vein-type	Ag–Pb–Zn–(Sn)	Ag:>2000 t@91 ~ 583 g/t, Pb:0.18Mt@1.56 ~ 11.37%, Zn:0.24Mt@0.85 ~ 6.96%	As above	As above	As above	As above	As above	As above
Jiaogenma (99°34', 30°24')	Batang, Sichuan	Hydrothermal vein-type	Sn	Sn:>90,000 t@0.6%	Upper Triassic sandstone, slate and carbonatite	K-feldspathization, greisenization, skarnization	Cassiterite, galena, sphalerite, stannite, pyrite, chalcopyrite, argentite	Ruoluolong and Rongyicuo biotite monzogranite	As above	As above
Cuomolong-Hailong (99°22', 30°30')	Batang, Sichuan	Skarn-type	Sn–Cu–Ag–Pb–Zn	Sn:36,011 t@0.1 ~ 18.25%, Cu@0.2 ~ 3.26%, Pb@0.12 ~ 7.95%, Zn@0.12% ~ 9.19, Ag@38.6 ~ 154 g/t	Upper Triassic sandstone, slate and carbonatite	K-feldspathization, greisenization, skarnization, silicification	Cassiterite, galena, sphalerite, bornite, chalcocite, pyrite, chalcopyrite	Ruoluolong and Cuomolong biotite monzogranite	Rb–Sr isochronal ages of Ruoluolong monzogranite: 93 ± 7 Ma	Zhang (1994), Qu et al. (2002), Fan (2009).
Lianlong (99°20', 30°32')	Baiyu, Sichuan	Skarn-type	Sn–Ag	Sn:27,000 t@0.45 ~ 1.62%, Ag:124 t@ 57.6 g/t	Upper Triassic sandstone, slate, pyroclastic and carbonatite	K-feldspathization, skarnization, greisenization, sericitization, marbleization	Cassiterite, galena, sphalerite, pyrite, chalcopyrite, stannite, pavonite	Lianlong biotite monzogranite	Rb–Sr isochronal ages of monzogranite: 89.1 ± 5.2 Ma	Qu et al. (2001), Qu et al. (2002)
Zhalong	Shiqu, Sichuan	Hydrothermal vein-type	Sn	No data	Upper Triassic sandstone and slate	greisenization, sericitization, silicification, chloritization	Cassiterite, galena, sphalerite, arsenopyrite, chalcopyrite	Zhalong granite porphyry	Rb–Sr isochronal ages of monzogranite: 103.7 ± 6.4 Ma	Qu et al. (2002)

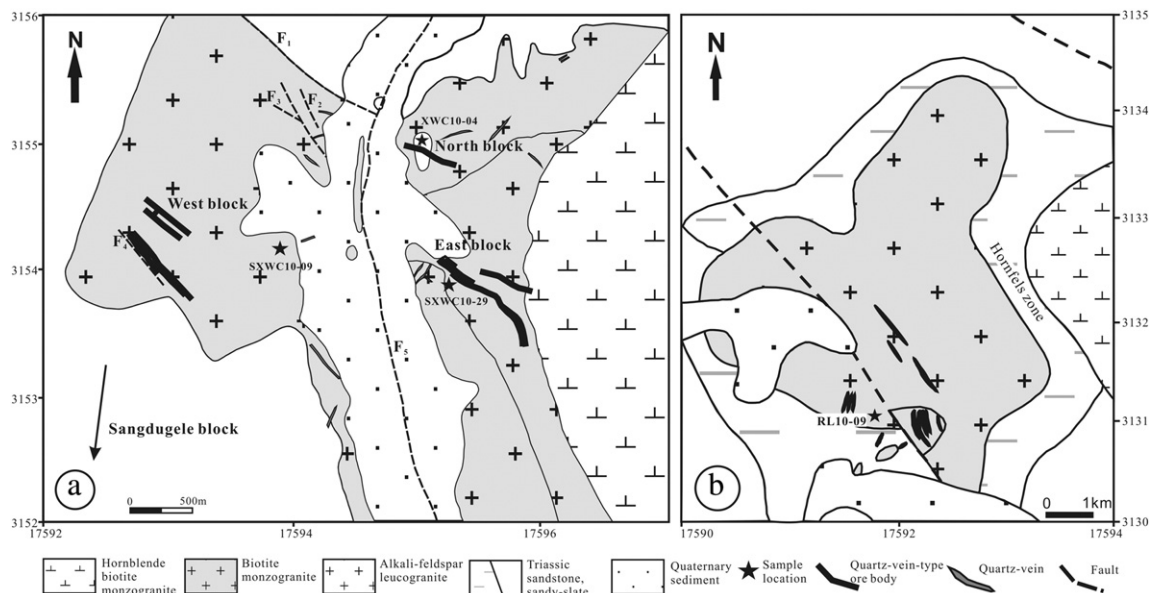


Fig. 2. Simplified geological map of (a) the Xiuwacu hydrothermal vein-type Mo-W deposit (modified after an unpublished exploration report from the Department of Land Resources in the Yunnan Province), and (b) Relin hydrothermal vein-type Mo-W deposit modified after Yin et al. (2009).

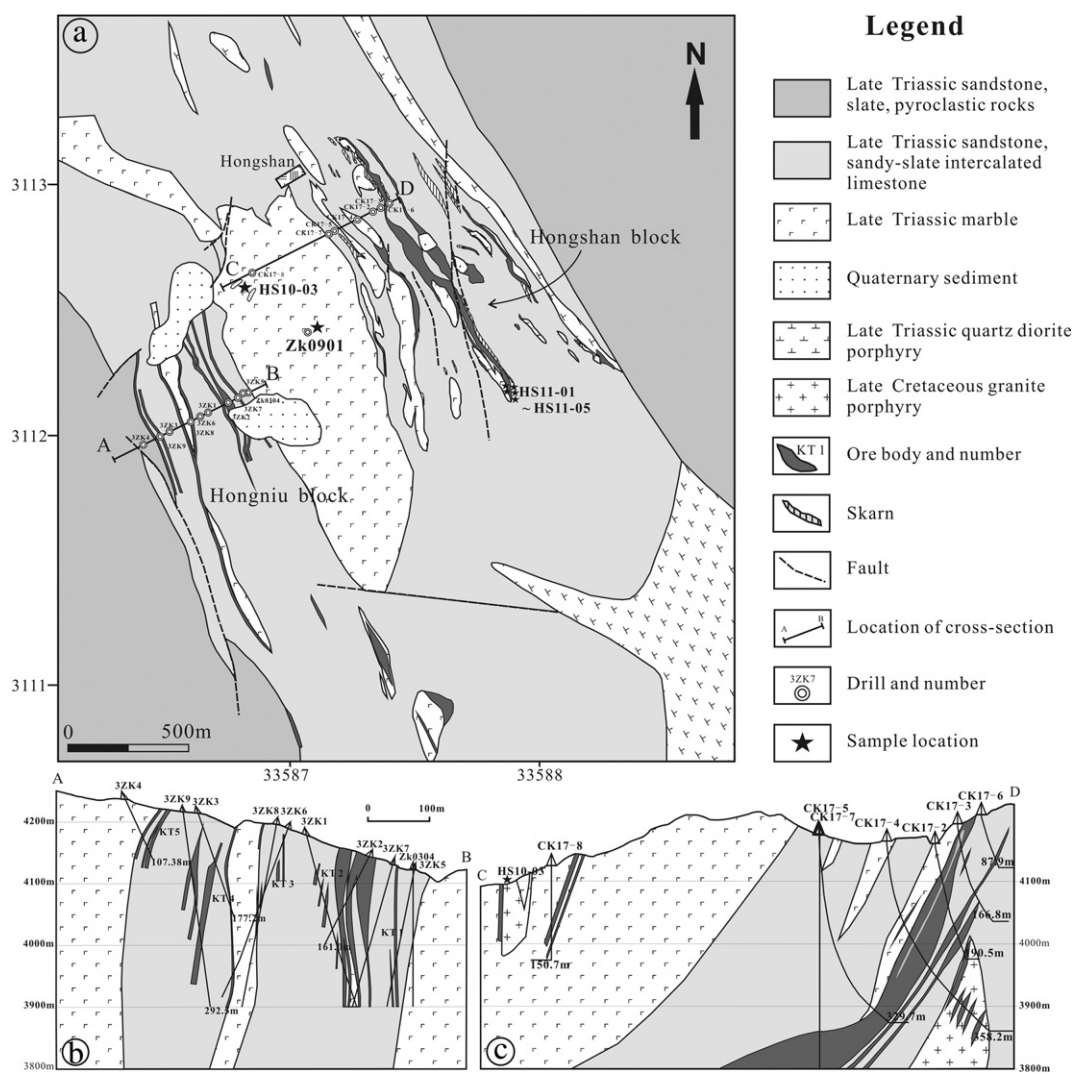


Fig. 3. Simplified geological map and cross-section of the Hongshan Cu–Mo deposit (modified after an unpublished exploration report from the Department of Land Resources in the Yunnan Province).

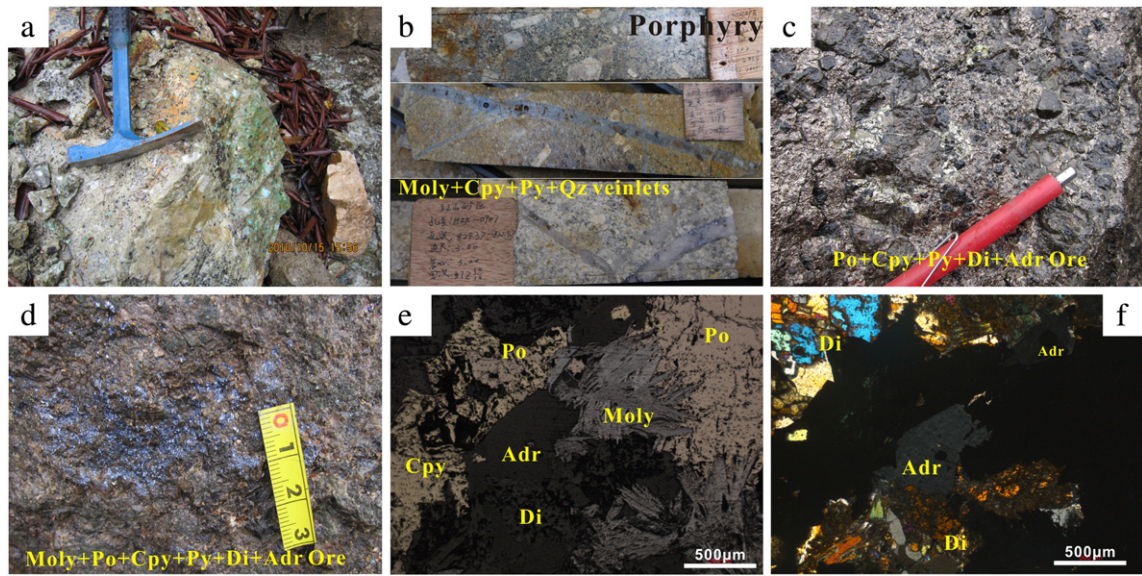


Fig. 4. Field photographs and reflected light photomicrographs of the intrusions and ores in the Hongshan Cu–Mo deposit. (a) Weak skarn alteration and chalcopyrite mineralization of granitic porphyry; (b) granitic porphyry associated with molybdenite–chalcopyrite–pyrite–quartz veinlets; (c) andradite–diopside–chalcopyrite–pyrite–pyrrhotite ore with chalcopyrite–pyrite zoning texture; (d) molybdenite–chalcopyrite–pyrite–pyrrhotite–andradite–diopside ore; (e) and (f) represent reflected light and crossed polarizer photomicrographs of the ore shown in (d) where molybdenite, chalcopyrite, pyrrhotite, andradite, and diopside coexist. Abbreviations for minerals are Di: diopside; Adr: andradite; Cpy: chalcopyrite; Moly: molybdenite; Po: pyrrhotite; Py: pyrite; and Qz: quartz.

3.3. Hongshan Cu–Mo deposit

The Hongshan Cu–Mo deposit lies ~30 km NE of Shangri-La City (Fig. 1c). Resources of Cu in the area amount to 0.64 Mt (average grade: 1.23%). In addition, the accompanying W, Mo, Ag, In, Co, and Bi amount to a total of more than 22,347 t (Table 1). The Hongshan deposit

is divided into two ore blocks: Hongshan and Hongniu (Fig. 3a). In the mining area, there are Late Triassic diorite porphyry in the west and Late Cretaceous granitic porphyry (Fig. 3a). The Late Triassic diorite porphyries have whole-rock Rb–Sr isochron ages and LA-ICP-MS zircon U–Pb ages of ~216 Ma (Huang et al., 2012; YBGM, 1990). Two small Late Cretaceous granitic porphyritic stocks have ages of ca. 81.1 Ma (Wang

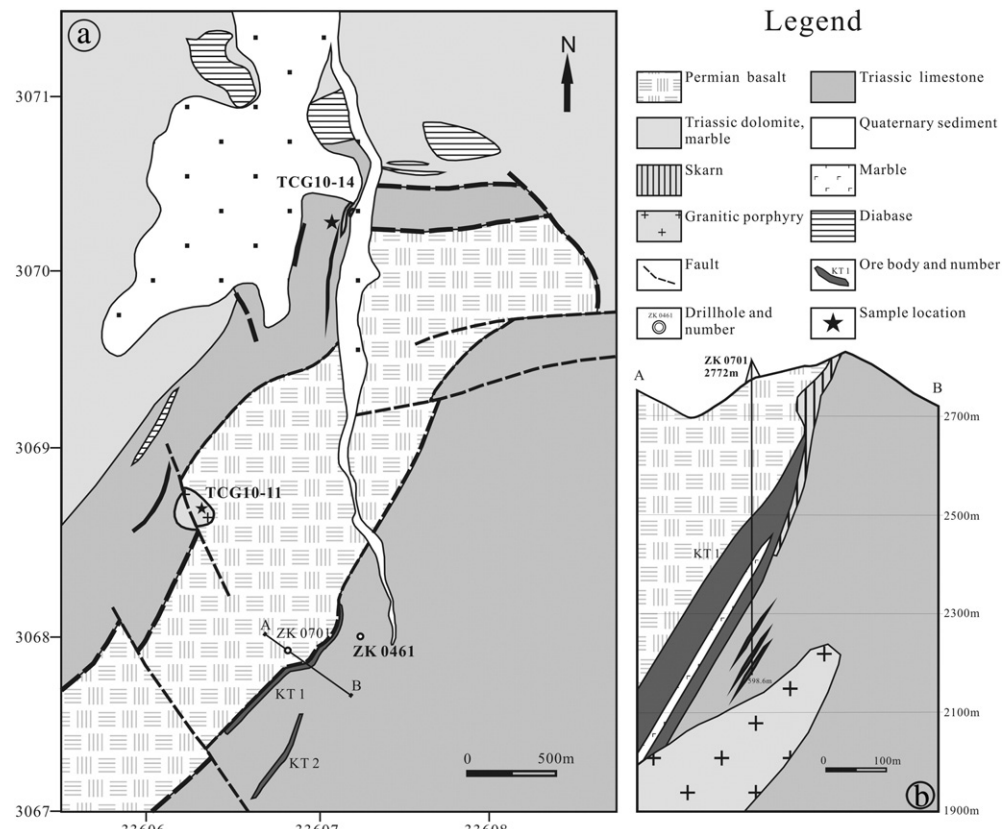


Fig. 5. Simplified geological map and cross-section map of the Tongchanggou Mo–Cu deposit (modified after Li et al., 2012).

et al., 2011b) and long axes spanning around 30 m, which are exposed in the Late Triassic marble on the surface. The stocks are weakly skarn and chalcopyrite altered (Fig. 4a). Most of the Late Cretaceous granitic porphyries and porphyry-type ore bodies are buried underneath the Triassic strata; these geological features were observed in three drill holes (CK17-4, CK17-7, and ZK-0901) (Fig. 3a; Huang et al., 2012; Xu et al., 2006; YBGMR, 1990). In drill hole CK17-4, granitic porphyries with porphyry type mineralization were found in the 250–350 m interval below the surface (Fig. 3c). Those porphyries and porphyry types of mineralization also occurred in the 817–899 m interval of drill hole ZK-0901 (Fig. 4b), and these were dated at ~76 Ma (LA-ICP-MS zircon U-Pb age) and ~80.2 Ma (molybdenite Re-Os age) (Huang et al., 2012; Li et al., 2011a), respectively. However, the extension of the granite porphyry and ore bodies at depth remains unknown. The mineralization style of the Hongshan deposit is usually divided into two: shallow skarn-type and vein-type Cu mineralization and deep porphyry-type Mo mineralization (Figs. 3a, 4b). Based on published geochronological results, some workers suggested that the shallow Cu mineralization occurring in the Late Triassic was related to the Triassic diorite porphyries intrusion, and the deep porphyry-type Mo mineralization during the Late Cretaceous was associated with the Cretaceous granitic porphyries (Huang et al., 2012; Li et al., 2011a; Wang et al., 2011b; Xu et al., 2006, 2012b). Detailed geological descriptions of the two parts are given below.

Nine main ore bodies are exposed in the shallow part of the Hongshan deposit far from the intrusions (Fig. 3a). The hanging walls are composed of Late Triassic sandy-slate, limestone, marble, and sandy-slate interbedded with marble. Most of the ore bodies are of the skarn-type with minor bodies of the veinlets-type, banded-type, and quartz-vein-type (Fig. 4c-d). These were mainly developed in the sandy-slate and marble contact zone, northwest (NW) trend, and southwest (SW) dip (dip angle: 60°–80°), and they were controlled by high-angle north-northwest (NNW)-strike faults. The skarn-type mineralization was developed close to the marble side in the contact zone, but veinlets-type and quartz-vein-type mineralization mainly occurred in the hornfelsic sandy-slate side. Ore textures are of a pyrite–chalcopyrite zoning texture (Fig. 4c), metasomatic texture, and granular texture. Ore minerals are composed of pyrrhotite, chalcopyrite, pyrite, molybdenite, sphalerite, galena, wolframite, scheelite, bismuthinite, tennantite, and bornite. Gangue minerals present included andradite, diopside, tremolite, quartz, and calcite.

Deep porphyry-type Mo mineralization was mainly developed within the granite porphyry (Fig. 3c). The ore bodies are mainly of the veinlet-type, disseminated-type, and quartz-vein-type (Fig. 4b). The ore minerals present here are molybdenite, pyrrhotite, chalcopyrite, and pyrite.

3.4. Tongchanggou Mo–Cu deposit

The Tongchanggou Mo–Cu deposit is located ~15 km southeast of Shangri-La City (Fig. 1c). The deposit has estimated resources of 50 Kt Mo (average grade: 0.3%), 34 Kt Cu (average grade: 0.8%), and 35 t Ag (average grade: 8.05 g/t) (Table 1). The strata in the Tongchanggou area consist of Triassic limestone and marble and Permian basalt interbedded with volcanic breccias. The Late Cretaceous biotite monzogranite and biotite granitic porphyry intruded into these strata and are

exposed in the western and northern portion of the mining area (Fig. 5a). Generally, skarn-type Mo–Cu mineralization occurred at shallower depths than porphyry-type Mo mineralization in the Tongchanggou deposit (Fig. 5b), which is similar to the mineralization characteristics of the Hongshan deposit. The depth extent of the porphyry and ore bodies remains uncertain at the present time.

Skarn-type Cu–Mo mineralization displays obvious vertical zoning, which is characteristic of the copper mineralization above the molybdenum mineralization. The ore bodies were situated along the contact zone between the Triassic limestone and Permian basalt, but they mainly occurred in the limestone and away from the biotite monzogranite (Fig. 5b). The attitudes of the ore bodies are consistent with the NE-trending and NW-dipping faults, with dip angles of 53°–79°. Ore structures are dominated by veinlets and disseminated mineralization. Ores are mainly metasomatic and granular. Ore minerals present included molybdenite, chalcopyrite, pyrite, magnetite, and scheelite. Furthermore, oxidation and carbonatization formed azurite, malachite, limonite, and molybdate. Gangue minerals present included andradite, diopside, tremolite, quartz, dolomite, and calcite.

The deep porphyry-type Mo mineralization is mainly hosted in the biotite monzogranite and within the contact zone with the marble (Fig. 5b). The ore bodies are mainly of the veinlet-type, disseminated-type, and quartz-vein-type. The ore minerals present included molybdenite, pyrrhotite, chalcopyrite, pyrite, and minor scheelite.

4. Samples and analytical methods

4.1. Molybdenite Re–Os dating

Five molybdenite samples collected from the ore body III (HS11-01 to HS11-05) in the Hongshan deposit (Fig. 3a; Table 2) were selected for Re–Os isotopic dating. Molybdenite grains are fine (0.02 to 1 mm) (Fig. 4d-f) and platy. They are disseminated in the skarn-type ores and coexisted with pyrrhotite and chalcopyrite (Fig. 4d-f). A heavy liquid separation method was first applied to separate molybdenite from the finely crushed (80–100 mesh) mineralized rocks. Then, molybdenite grains were handpicked individually under a binocular microscope to get molybdenite separates of over 99% purity.

Molybdenite Re–Os isotope analyses were conducted at the State Key Laboratory of Ore Deposit Geochemistry (SKLODG), Institute of Geochemistry, Chinese Academy of Sciences, Guiyang (IG-CAS). Ten milligrams of molybdenite were accurately weighed and transferred to a Carius tube. The Carius tube was then cooled with an ice water bath, and appropriate volumes of weighed ^{185}Re and ^{190}Os spikes and 5 mL of cooled HNO_3 (~25 °C, in refrigerator) were added. The sealed Carius tube was placed in a stainless steel jacket and heated to 180 °C for about 12 h. After slowly cooling down in air to room temperature, the Carius tube was further cooled in a refrigerator for 2 h. Then, Os was distilled in situ from the solution in the Carius tube by the distillation system described in Qi et al. (2010); Os was trapped with 1.5 mL of a 5% HCl solution. After the distillation, Re was separated from the residual solution following the method of Qi et al. (2004). Finally, the Re and Os isotope ratios in the two solutions were analyzed with a PerkinElmer ELAN DRC-e ICP-MS. Average blanks

Table 2

Description of dated samples and their ages in this study.

Sample	Pluton	Lat (°)	Long (°)	Rock description	Weighted mean ages (Ma)	Reference
SXWC10-09	Xiuwacu	28.498	99.961	Medium grained monzogranite	84.8 ± 0.6	This study
SXWC10-29		28.496	99.970	Medium grained biotite monzogranite	85.6 ± 0.5	
XWC10-04		28.505	99.970	Fine grained alkali-feldspar leucogranite	84.4 ± 1.4	
RL10-09	Relin	28.290	99.939	Coarse grained biotite monzogranite	82.7 ± 0.5	
TCG10-11	Tongchanggou	27.725	100.076	Medium grained biotite monzogranite	87.4 ± 0.6	
TCG10-14		27.739	100.075	Medium grained biotite monzogranite	86.3 ± 0.6	
HS11-01–05	Hongshan	28.123	99.891	Molybdenite from skarn type ores	81.2 ± 2.6	
HS10-03		28.122	99.877	Medium grained granitic porphyry	81.1 ± 0.5	Wang et al., 2011b

Table 3

Molybdenite Re–Os analytical results for skarn-type mineralization in Hongshan deposit.

Sample	Sample wt.(mg)	Re(ppm)	$^{187}\text{Re}(\text{ppm})$	$^{187}\text{Os}(\text{ppb})$	Data(Ma)
HS11-01	10.6	36.7 ± 0.8	23.0 ± 0.5	30.6 ± 0.3	80.3 ± 0.8
HS11-02	10.8	66.1 ± 1.8	41.4 ± 1.5	53.8 ± 0.4	78.3 ± 0.6
HS11-03	10.7	19.7 ± 0.3	12.3 ± 0.2	16.9 ± 0.2	82.2 ± 1.2
HS11-04	10.6	80.6 ± 0.5	50.5 ± 0.3	69.0 ± 0.7	82.3 ± 0.8
HS11-05	10.7	47.7 ± 1.2	29.8 ± 0.8	39.4 ± 0.8	79.4 ± 1.7

Note: Decay constant: $\lambda(^{187}\text{Re}) = 1.666 \times 10^{-11}\text{a}^{-1}$ (Smoliar et al., 1996). Uncertainties are absolute at 1σ with uncertainty on Re and ^{187}Os concentrations and in the ^{187}Re decay constant.

for this analysis were 6.4 ± 1.0 pg for Re and 2.0 ± 0.4 pg for Os, which was negligible in relation to the measured Re and Os abundances. The analytical reliability was verified by repeated analyses of molybdenite standard HLP (Du et al., 2004). The average Re–Os age for HLP was determined to be 223.1 ± 3.4 Ma (95% confidence level), which is consistent with the certified age of 221.4 ± 5.6 Ma (Du et al., 2004). The molybdenite model ages were calculated by using an equation of $t = [\ln(1 + ^{187}\text{Os}/^{187}\text{Re})]/\lambda$, where λ is the ^{187}Re decay constant of $1.666 \times 10^{-11}\text{ yr}^{-1}$ (Smoliar et al., 1996). The ^{87}Re – ^{87}Os isochron diagram was plotted by use of the Isoplot program of Ludwig (2003).

4.2. Zircon U–Pb dating

Samples were collected separately from granitic intrusions in the Xiuwacu, Relin, and Tongchanggou deposits, which are all spatially associated with mineralization. The sample locations are shown in Figs. 2 and 5. Samples SXWC10-09 and SXWC10-29 from the Xiuwacu area were collected from the medium-coarse grained monzogranite and biotite monzogranite in the west and east block, respectively; sample XWC10-04 was collected from the fine grained alkali-feldspar leucogranite in the north block. In the Relin area, sample RL10-09 was collected from the coarse-grained biotite monzogranite in the west of the deposit. In the Tongchanggou area, samples TCG10-11 and TCG10-14 were collected from the medium grained biotite monzogranite stock in the west and north of the mining area, respectively.

Zircons were separated from these above samples by using conventional heavy liquid and magnetic separation techniques. Representative zircon grains were handpicked under a binocular microscope and mounted in an epoxy resin disk, and then polished to about half their thickness for analysis. Zircons were documented with transmitted and reflected light micrographs as well as cathodoluminescence (CL) images to reveal their internal structures (Fig. 7). The CL images were obtained

by using an LEO1450VP scanning electron microscope at the Institute of Geology and Geophysics, Chinese Academy of Sciences, Beijing.

The U–Pb dating and trace element analyses of zircon were conducted with LA-ICP-MS at the State Key Laboratory of Geological Processes and Mineral Resources, China University of Geosciences, Wuhan. Detailed operating conditions for the laser ablation system and the ICP-MS instrument and data reduction are the same as those described previously (Liu et al., 2008, 2010). Laser sampling was performed by using a GeoLas 2005. An Agilent 7500a ICP-MS instrument was used to acquire ion-signal intensities. Helium was applied as a carrier gas. Argon was used as the make-up gas and mixed with the carrier gas via a T-connector before entering the ICP. Nitrogen was added into the central gas flow (Ar + He) of the Ar plasma to decrease the detection limit and improve precision (Hu et al., 2008). The size for each analysis spot was $32 \mu\text{m}$. Each analysis incorporated a background acquisition period of approximately 20–30 s (gas blank), which was followed by 50 s of data acquisition from the sample. The Agilent Chemstation was utilized for the acquisition of each individual analysis. Off-line selection and integration of background and analyte signals, and time-drift correction and quantitative calibration for trace element analyses and U–Pb dating were performed by ICPMSDataCal (Liu et al., 2008, 2010). Zircon 91500 was used as an external standard for U–Pb dating, and this was analyzed twice every five analyses. Time-dependent drifts of U–Th–Pb isotopic ratios were corrected using a linear interpolation (with time) for every five analyses according to the variations of 91500 (i.e., 2 zircon 91500 + 5 samples + 2 zircon 91500) (Liu et al., 2010). Preferred U–Th–Pb isotopic ratios used for 91500 were from Wiedenbeck et al. (1995). Uncertainty of the preferred values for the external standard 91500 was propagated to the ultimate results of the samples. The results of the standard zircons 91500 and GJ are listed in Appendix 1. Measured compositions were corrected for common Pb using the measured non-radiogenic ^{204}Pb . Concordia diagrams and weighted mean calculations were made using Isoplot/Ex_ver3 (Ludwig, 2003).

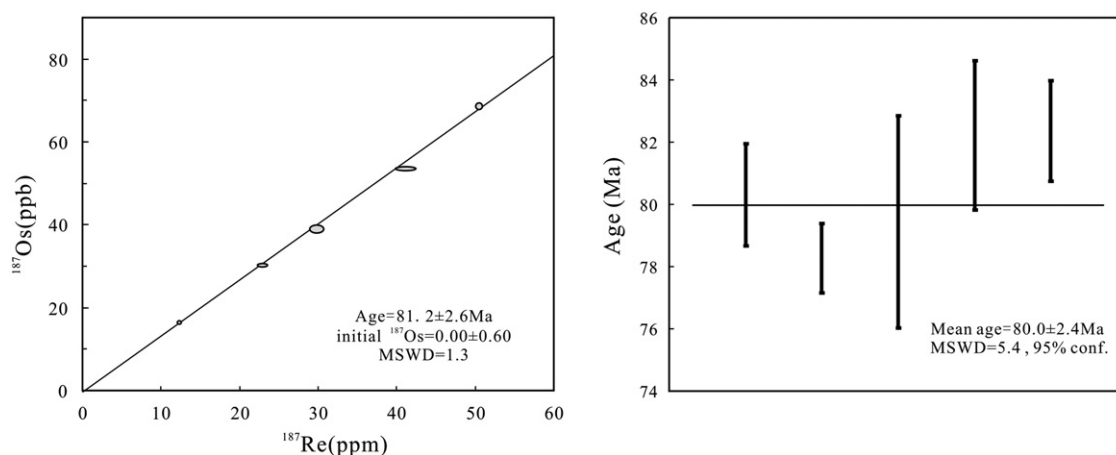


Fig. 6. (a) Re–Os isochron diagram and (b) weighted average model age diagram for the molybdenite samples from the Hongshan deposit.

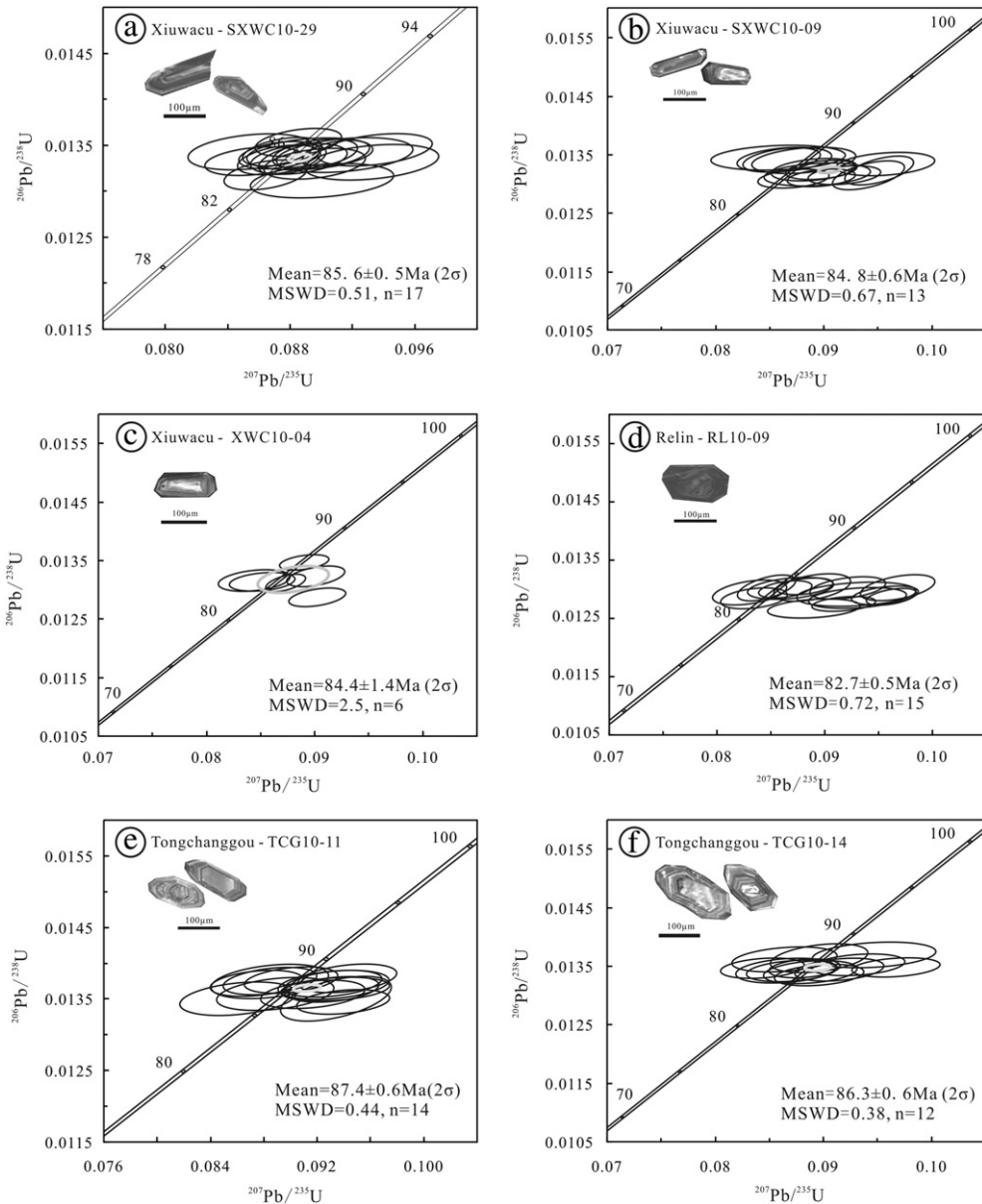


Fig. 7. Cathodoluminescence images of selected zircons and zircon U–Pb concordia diagrams for the samples from Xiuwacu, Relin, and Tongchanggou areas. The petrology and location of the samples are presented in Table 2.

4.3. Zircon Hf isotopic analytical methods

In situ zircon Hf isotopic analysis was carried out on a Nu plasma multi-collector ICP-MS equipped with a UP-213 laser-ablation system (LA-MC-ICP-MS) at IG-CAS. Most Lu-Hf isotopic measurements were made on the same domains previously analyzed for U-Pb dating. During the course of this study, a laser repetition rate of 10 Hz was used and beam diameters were 60 μm . Laser beam energy density was 5.27–6.15 J/cm². The detailed analytical procedures were similar to those described by Tang et al. (2008). Our determined $^{176}\text{Hf}/^{177}\text{Hf}$ ratios of 0.282309 ± 0.000024 (2σ , n = 19) for zircon standards 91500 are consistent with reported values for $^{176}\text{Hf}/^{177}\text{Hf}$ ratios of 0.282306 ± 0.000010 (2σ) by Woodhead et al. (2004).

4.4. Whole rock major and trace element analyses

All the studied samples (fresh) were collected from drill holes in the three different deposits. The detailed sample locations are given in

Table 4. Major elements were determined by using an Axios PW4400 X-ray fluorescence spectrometer (XRF) at SKLODG, IG-CAS, and fused lithium-tetraborate glass pellets were employed. The analytical precision is better than 5%. Trace elements were analyzed by using a PerkinElmer DRC-e ICP-MS at SKLODG. The powdered samples (50 mg) were dissolved in high-pressure Teflon bombs with a HF-HNO₃ mixture for 2 days at 190 °C. Rh was used as an internal standard to monitor signal drift during counting. The detailed analytical methods were given by Qi et al. (2000). The analytical precision is generally better than 10%.

5. Results

5.1. Molybdenite Re-Os ages

The analysis results are listed in Table 3. These samples have relatively high Re contents ranging from 19.7 ppm to 80.6 ppm. Five molybdenite Re-Os model ages vary from 78.3 ± 0.6 Ma to 82.3 ± 0.8 Ma with

a weighted mean average of 80.0 ± 2.4 Ma (MSWD = 5.4) (Fig. 6b). These samples yield a low initial ^{187}Os value of 0.0 ± 0.6 ppb indicating that the model ages for molybdenite are reliable. The ^{187}Re – ^{187}Os isochron age is 81.2 ± 2.6 Ma (MSWD = 1.3) (Fig. 6a), which is consistent with the model ages.

5.2. Zircon U–Pb ages

Most of the zircons from samples (SXWC10-29, SXWC10-09, XWC10-04, RL10-09, TCG10-11, and TCG10-14) in the Shangri-La region are colorless and euhedral with igneous oscillatory zoning; while the crystals from the sample RL10-09 are brown and translucent due to radioactive damage from their high-uranium contents (Li et al., 2007b). The zircon grains mainly vary from $60\ \mu\text{m}$ to $300\ \mu\text{m}$ in length and have length to width ratios of about 2:1 to 3:1. The results of the six samples and standards zircons (zircon 91500 and GJ-1) are given in Appendix 1.

Seventeen analyses of zircons from sample SXWC10-29 yield $^{206}\text{Pb}/^{238}\text{U}$ ages varying from 84.0 Ma to 86.6 Ma with a weighted mean $^{206}\text{Pb}/^{238}\text{U}$ age of 85.6 ± 0.5 Ma (2σ , MSWD = 0.51) (Fig. 7a). Thirteen analyses of sample SXWC10-09 yield $^{206}\text{Pb}/^{238}\text{U}$ ages range from 83.9 Ma to 86.1 Ma with a weighted mean age of 84.8 ± 0.6 Ma (2σ , MSWD = 0.67) (Fig. 7b). These two ages are consistent with each other within the range of analytical error, and interpreted to be the crystallization age of the biotite monzogranite intrusion at Xiuwacu. Six analyses from sample XWC10-04 were obtained. The $^{206}\text{Pb}/^{238}\text{U}$ ages vary from 82.4 Ma to 86.2 Ma, yielding a weighted mean age of 84.4 ± 1.4 Ma (2σ , MSWD = 2.5) (Fig. 7c); this reflects the crystallization age of the alkali-feldspar leucogranite intrusion at Xiuwacu.

Fifteen analyses of 15 zircons were obtained from sample RL10-09. The $^{206}\text{Pb}/^{238}\text{U}$ ages range from 81.2 Ma to 83.6 Ma, which yield a weighted mean age of 82.7 ± 0.5 Ma (2σ , MSWD = 0.72) (Fig. 7d); this is interpreted to be the crystallization age of the monzogranite intrusion at Relin.

Table 4

Major (wt.%) and trace elements (ppm) data for the Relin, Hongshan and Tongchanggou intrusions in the southern Yidun Arc.

Intrusions	Relin intrusion							Hongshan intrusion		Tongchanggou intrusion					
	Sample no.	RL12-01	RL12-03	RL12-04	RL12-05	RL12-06	RL12-07	RL12-08	HS12-05	HS12-051	TCG12-05	TCG12-08	TCG12-09	TCG12-10	TCG12-13
Drill hole no.	ZK0002							ZK0901		ZK0461					
Location	536 m 480 m 489 m 465 m 474 m 340 m 360 m							832 m	890 m	480 m	550 m	568 m	561 m	596 m	606 m
Rock type	Monzogranitic porphyry							Granitic porphyry		Biotite monzogranite					
SiO ₂	69.8	69.8	69.4	70.0	68.8	70.0	69.2	68.3	68.3	67.3	66.3	65.7	65.6	65.2	66.3
Al ₂ O ₃	14.1	14.2	15.0	13.7	14.9	14	14.7	13.6	13.6	15.2	15.3	15.0	14.6	14.8	14.7
Fe ₂ O ₃ T	2.83	3.16	2.86	3.44	2.70	3.07	2.89	3.83	3.83	3.14	3.19	3.37	3.27	3.29	2.97
MgO	0.83	0.99	0.92	1.06	0.83	0.88	0.86	0.77	0.77	1.15	1.25	1.44	1.27	1.29	1.17
CaO	1.80	2.37	2.37	2.20	2.21	2.20	2.31	1.50	1.50	2.61	2.20	2.51	2.96	3.09	2.86
Na ₂ O	3.26	3.84	4.05	3.58	3.93	3.66	3.81	3.16	3.16	3.79	3.70	3.56	3.53	3.52	3.63
K ₂ O	5.42	3.97	4.08	4.24	4.52	4.16	4.48	5.44	5.44	3.82	3.54	3.94	3.77	3.69	3.74
P ₂ O ₅	0.19	0.21	0.19	0.23	0.18	0.19	0.19	0.23	0.23	0.24	0.27	0.26	0.26	0.27	0.24
TiO ₂	0.46	0.54	0.46	0.55	0.44	0.47	0.50	0.50	0.50	0.49	0.55	0.52	0.53	0.54	0.50
MnO	0.03	0.04	0.03	0.04	0.03	0.03	0.03	0.05	0.05	0.04	0.02	0.04	0.03	0.05	0.03
LO.I.	0.60	0.69	0.56	0.70	0.73	0.75	0.71	1.67	1.67	1.75	2.93	3.07	3.58	3.47	3.39
Tatol	99.4	99.9	100	99.8	99.4	99.5	99.8	99.1	99.1	99.7	99.4	99.6	99.7	99.4	99.7
Mg#	37	38	39	38	38	36	37	28	28	42	44	46	43	44	44
Cr	16.8	17.7	15.3	16.0	15.0	15.6	17.6	19.9	21.3	14.4	17.7	22.2	19.1	20.4	14.3
Ni	6.20	7.77	6.51	8.05	6.21	7.19	7.99	6.67	6.73	7.66	8.25	8.98	9.23	8.28	9.74
Ga	19.1	19.9	18.6	19.4	20.6	20.3	21.3	21.1	21.0	20.5	21.7	21.7	20.4	18.8	19.3
Rb	293	226	210	255	243	237	254	209	210	152	191	169	182	162	186
Sr	386	421	387	363	439	385	425	483	487	726	515	698	905	705	850
Y	14.0	16.6	12.4	16.3	13.1	15.1	15.8	17.0	16.9	11.9	12.3	11.6	12.8	13.4	11.8
Zr	195	208	180	230	196	207	208	232	244	165	181	171	177	167	171
Nb	40.9	44.0	36.7	46.2	35.6	43.0	46.8	39.8	40.7	35.5	36	34.3	37.0	33.8	32.6
Ba	1010	625	592	698	894	641	828	684	680	1210	950	1320	1340	1270	1510
La	56.4	63.7	47.0	65.0	54.5	55.4	53.0	58.5	57.8	59.1	65.7	58.8	64.9	62.9	70.7
Ce	97.9	110	84.0	114	94.5	97.8	94.8	122	121	99.4	112	99.8	110	104	113
Pr	9.59	10.8	8.20	10.9	9.00	9.48	9.27	12.5	12.4	9.37	10.5	9.65	10.4	10.2	10.7
Nd	30.9	36.8	26.9	35.9	29.4	31.3	31.5	41.2	41.2	30.1	34.1	31.1	33.7	33.7	35.1
Sm	4.77	5.48	4.07	5.4	4.33	4.71	4.95	5.97	5.84	4.31	4.85	4.53	5.11	4.89	4.90
Eu	1.08	1.29	0.93	1.19	1.15	1.08	1.13	1.35	1.37	1.24	1.31	1.31	1.3	1.31	1.21
Gd	3.87	4.56	3.26	4.52	3.69	3.9	4.14	4.51	4.72	3.42	3.85	3.53	3.87	3.81	3.69
Tb	0.54	0.63	0.45	0.58	0.47	0.52	0.56	0.62	0.61	0.45	0.49	0.45	0.50	0.53	0.50
Dy	2.51	2.99	2.23	3.04	2.32	2.67	2.73	2.81	2.84	2.15	2.25	2.17	2.35	2.48	2.20
Ho	0.48	0.58	0.43	0.57	0.45	0.51	0.54	0.53	0.40	0.40	0.40	0.38	0.42	0.47	0.43
Er	1.38	1.69	1.18	1.60	1.31	1.46	1.55	1.51	1.46	1.11	1.20	1.11	1.17	1.37	1.22
Tm	0.20	0.24	0.18	0.21	0.18	0.21	0.21	0.20	0.21	0.15	0.16	0.15	0.18	0.19	0.17
Yb	1.30	1.56	1.20	1.59	1.21	1.47	1.45	1.41	1.34	0.98	0.97	1.01	1.12	1.23	1.02
Lu	0.21	0.24	0.19	0.25	0.18	0.23	0.25	0.21	0.21	0.15	0.15	0.16	0.15	0.18	0.16
Hf	5.52	5.56	5.07	6.23	5.25	5.82	5.62	5.84	6.08	4.19	4.59	4.27	4.56	4.72	4.69
Ta	2.92	3.08	2.59	3.18	2.36	2.97	3.4	2.15	2.09	1.95	2.03	1.86	2.08	1.99	1.98
Pb	19.6	17.8	16.4	17.5	18.4	16.1	17.9	19.3	19.5	19.0	11.4	14.3	15.3	14.9	14.9
Th	29.6	30.4	24.8	32.8	25.4	27.0	26.1	28.1	28.5	19.5	19.4	19.1	20.3	20.1	20.8
U	16.0	14.2	13.2	17.4	11.6	14.7	14.3	7.23	7.36	7.54	4.12	6.06	6.18	6.54	6.56
Sr/Y	28	25	31	22	34	25	27	28	29	61	42	60	71	53	72
La/Yb	43	41	39	41	45	38	37	41	43	60	68	58	58	51	69
δEu	0.74	0.77	0.75	0.72	0.86	0.75	0.74	0.76	0.77	0.95	0.9	0.97	0.86	0.9	0.83

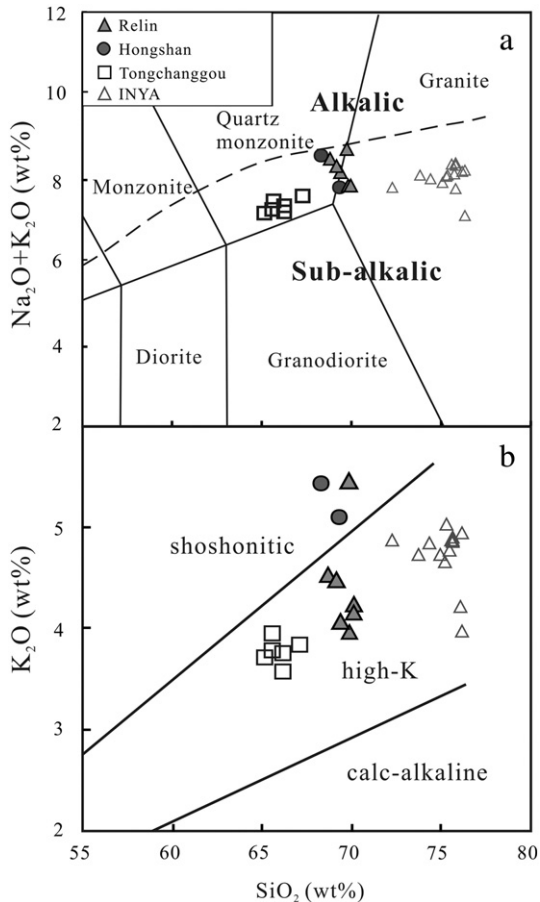


Fig. 8. (a) Total alkali versus SiO₂ diagram; (b) K₂O versus SiO₂ diagram for Late Cretaceous intrusions in the Yidun Arc. Reference fields are from Middlemost (1994) and Peccerillo and Taylor (1976), respectively. The INYA stands for Late Cretaceous A-type granites in the northern Yidun Arc from Qu et al. (2002).

Fourteen and 12 analyses were conducted for samples TCG10-11 and TCG10-14, respectively. The ²⁰⁶Pb/²³⁸U ages of the zircons from sample TCG10-11 vary from 86.2 to 88.3 Ma, which yield a

weighted mean age of 87.4 ± 0.6 Ma (2σ , MSWD = 0.44) (Fig. 7e). The ²⁰⁶Pb/²³⁸U ages of the zircons from sample TCG10-14 vary from 85.5 Ma to 87.7 Ma, which gave a weighted mean age of 86.3 ± 0.6 Ma (2σ , MSWD = 0.39) (Fig. 7f). These two ages are interpreted as the crystallization ages of the biotite monzogranite at Tongchanggou.

5.3. Zircon Hf isotopes

Zircons from samples RL10-09, HS10-03, and TCG10-11 were analyzed for Lu-Hf isotopes, mostly on the same grains dated by U-Pb previously. The results are listed in Appendix 2. Twenty analyses of sample RL10-09 (82.7 Ma) yield $\epsilon_{\text{Hf}}(t)$ values between -7.1 and -4.1 with T_{DM2} model ages of 1.41–1.59 Ga. Eighteen analyses of sample HS10-03 (81.1 Ma) yield $\epsilon_{\text{Hf}}(t)$ values ranging from -7.9 to -5.1 with T_{DM2} model ages of 1.47–1.64 Ga. Twenty analyses of sample TCG10-11 (87.4 Ma) yield $\epsilon_{\text{Hf}}(t)$ values between -4.9 and -2.3 with T_{DM2} model ages of 1.29–1.49 Ga.

5.4. Major and trace elements

Major and trace elemental data for the Relin, Hongshan, and Tongchanggou intrusions are listed in Table 4. These three intrusions have similar geochemical compositions with SiO₂ ranging from 65.2 wt.% to 70.0 wt.%. In the TAS (total alkali versus SiO₂) diagram, most of the samples are sub-alkalic and fall into the field of quartz monzonite (Fig. 8a). These samples have relatively low MgO (0.66–1.44 wt.%) and Mg# (25–46), and high K₂O (3.54–5.44 wt.%) and K₂O/Na₂O (1.0–1.9) (Figs. 8b and 11d). They are metaluminous and slightly peraluminous (Al₂O₃ = 13.6–15.3 wt.%; A/CNK = 0.94–1.12, mostly <1.0).

In the chondrite-normalized rare earth element diagram, all the rocks are depleted in heavy rare earth elements (HREEs) relative to light rare earth elements (LREEs) (La/Yb = 26–50) with negligible Eu anomalies (Eu/Eu* = 0.72–0.97) (Fig. 9a). In the trace element spider diagram, all the samples are enriched in Rb (152–294 ppm), Th (19.1–45.9 ppm), and U (6.06–17.4 ppm), and relatively depleted in Nb (32.6–46.8 ppm), Ta (1.86–3.40 ppm), Ti (0.44–0.55 wt.%), and P (0.18–0.27 wt.%) (Fig. 9b). In addition, they had high Sr (363–905 ppm), and low Y (11.6–17.0 ppm) and Yb (0.97–1.41 ppm).

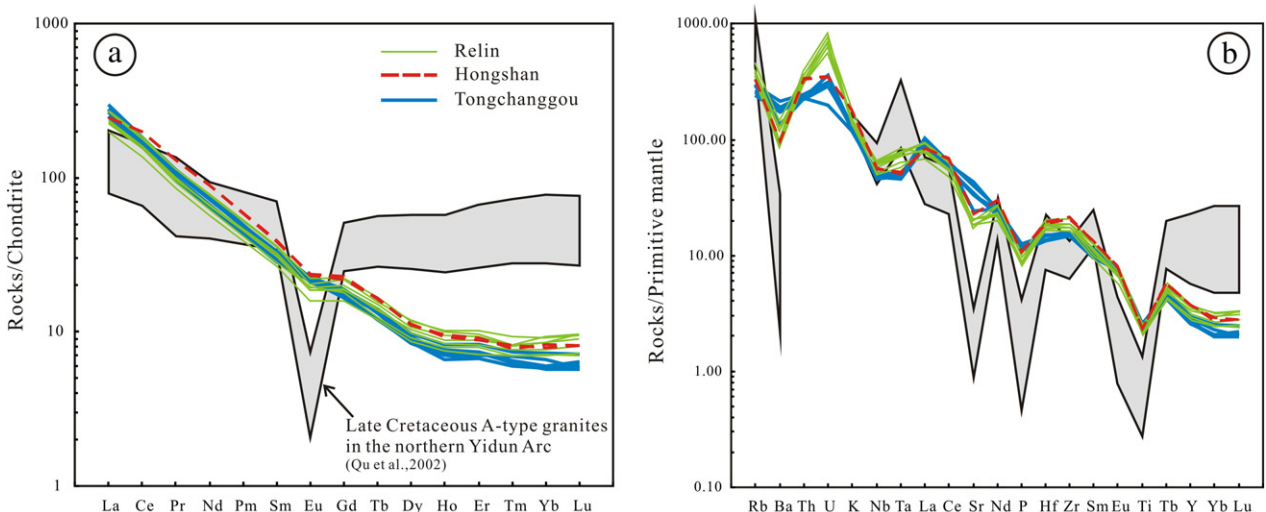


Fig. 9. (a) Chondrite-normalized rare earth elements (REEs) and (b) primitive mantle-normalized trace elemental spider diagrams for intrusions in the Yidun Arc. Chondrite normalizing values and primitive mantle values follow Sun and McDonough (1989).

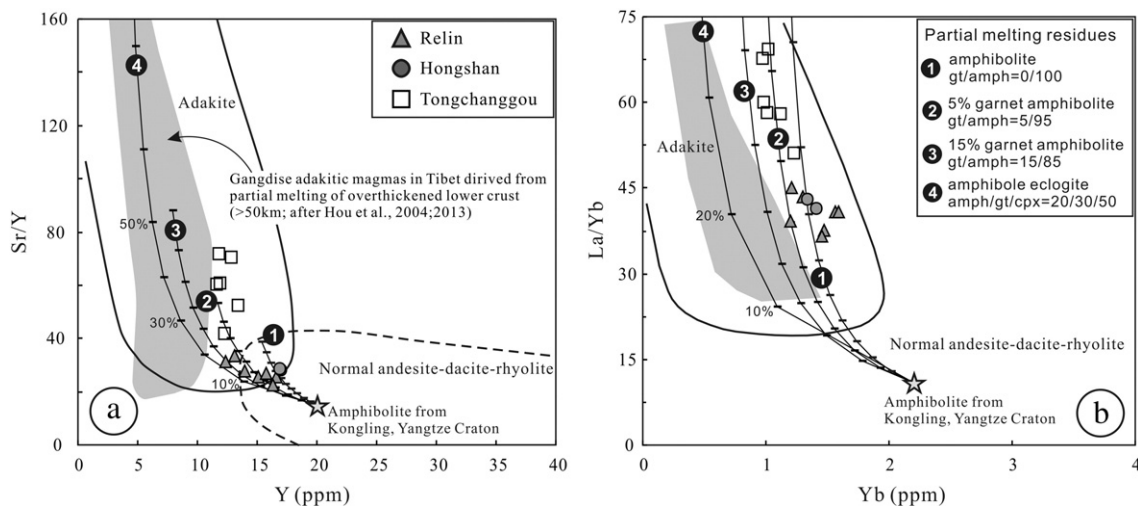


Fig. 10. (a) Sr/Y versus Y and (b) La/Yb versus Yb diagrams for intrusions in the Yidun Arc showing the results of batch-melting modeling. For trace element modeling, we applied the Shaw's batch melting equation $C_L = C_0/[F + D(1 - F)]$ (Shaw, 1970), where C_0 and C_L are trace element abundances in the source and liquid, respectively, D means bulk partition coefficients, and F denotes degree of partial melting. The partition coefficients were taken from the GERM Kd database (Qian and Hermann, 2013). The four dashed curves represent melting leaving a restite of amphibole eclogite, 10% garnet amphibolite, 5% garnet amphibolites, and garnet-free amphibolite, respectively (after Lu et al., 2013); values are based on average values of amphibolite from Kongling, Yangtze Craton as the starting composition ($Sr = 300$ ppm, $Y = 20$ ppm, $La = 20$ ppm, $Yb = 2.2$ ppm; Gao et al., 1999). Adakite fields are from Richards and Kerrich (2007) and Castillo et al. (1999).

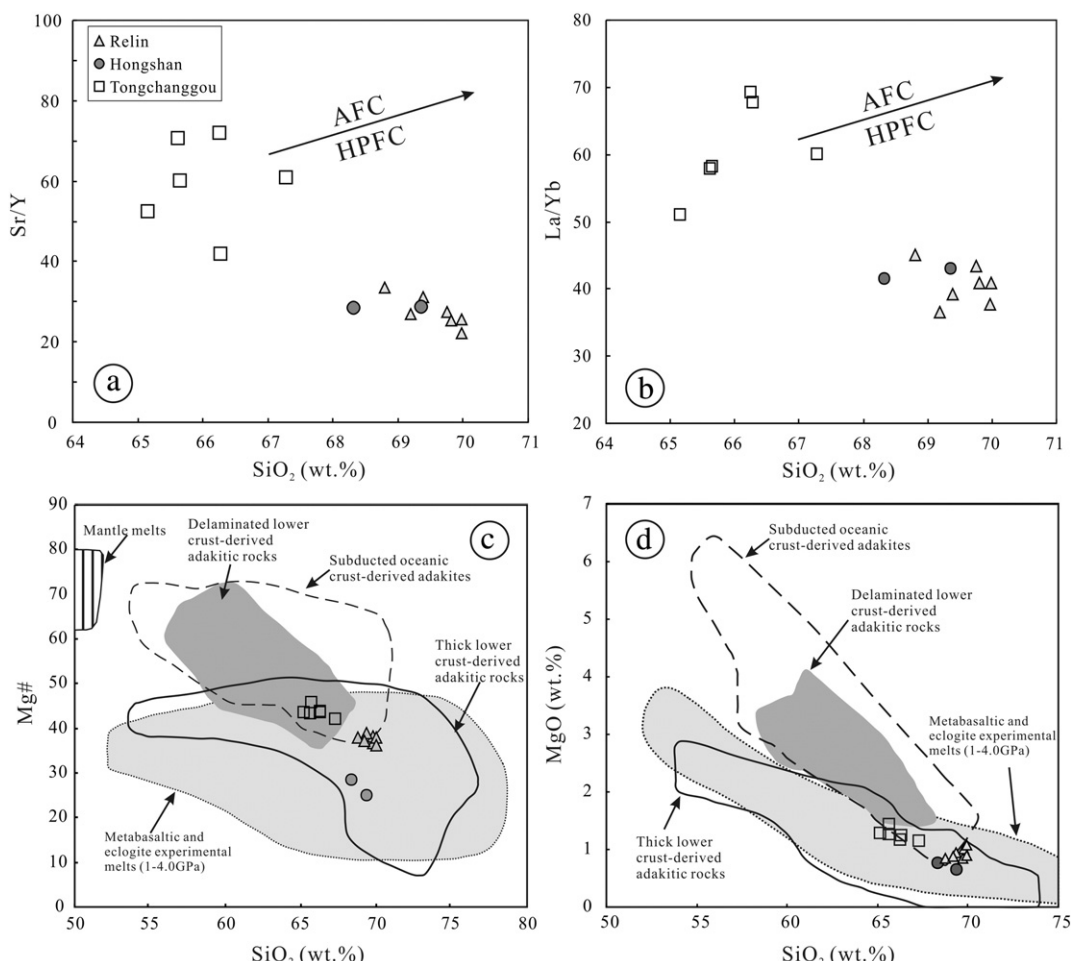


Fig. 11. (a) Sr/Y versus SiO₂ diagram; (b) La/Yb versus SiO₂ diagram; (c) Mg# versus SiO₂ plot [$Mg\# = 100 \times \text{molar Mg}/(\text{Mg} + \text{Fe})$]; and (d) MgO versus SiO₂ diagram for the intrusions in the southern Yidun Arc. Reference fields for (c) and (d) are from Wang et al. (2006).

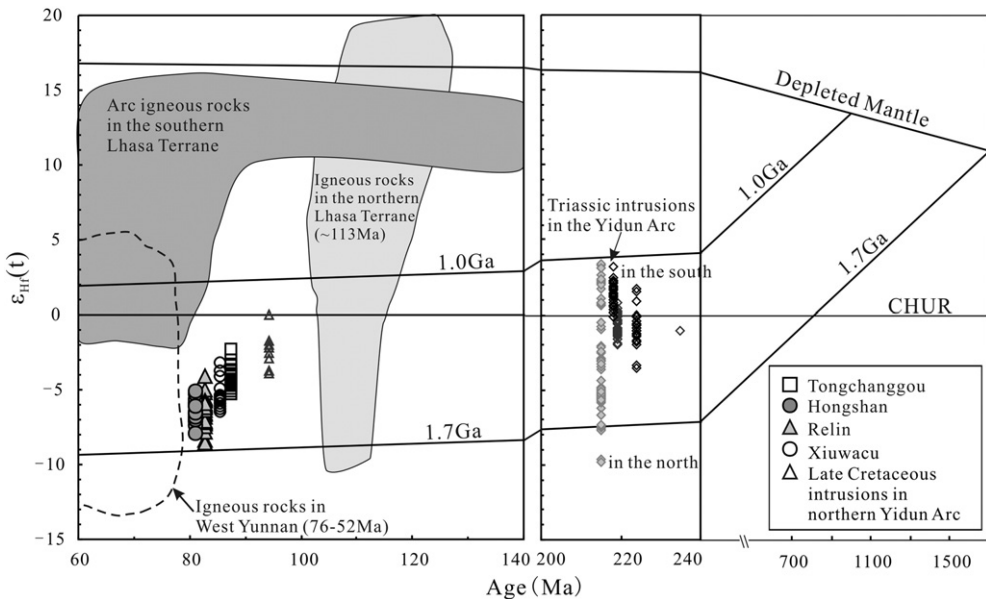


Fig. 12. T- $\epsilon_{\text{Hf}}(t)$ diagram for the intrusions in the southern Yidun Arc. Samples of the Xiuwacu intrusion are from our unpublished data; samples of Late Cretaceous intrusions in the northern Yidun Arc are from Reid et al. (2007); field of arc igneous rocks in the southern Lhasa Terrane and igneous rocks in the northern Lhasa Terrane (~113 Ma) are from Zhu et al. (2011a); field of igneous rocks in the West Yunnan (76–52 Ma) are from Xu et al. (2012c); and Late Triassic intrusions in the northern and southern Yidun Arc are from three previous studies (He et al., 2013; Leng et al., 2012; Liu and Li, 2013).

6. Discussion

6.1. Timing of and relationship between mineralization and magmatism in the Southern Yidun Arc

6.1.1. Age of the Hongshan deposit

Many studies have shown that the molybdenite Re-Os system is a remarkably robust tool for dating because it is not affected by late hydrothermal, metamorphic, and/or tectonic events (Selby et al., 2003; Stein et al., 2001), given that the Re-Os closure temperature for molybdenite is up to 500 °C (Suzuki et al., 1996). Therefore, the molybdenite Re-Os dating has been used for dating primary sulfide mineralization (Mao et al., 2008; Selby et al., 2003; Stein et al., 1997). Moreover, geologically young and naturally fine-grained molybdenites may have little ^{187}Re - ^{187}Os decoupling effects, and small quantities of the molybdenite can deliver reliable Re-Os ages (Selby and Creaser, 2004).

Xu et al. (2006) and Li et al. (2011a) reported molybdenite ^{187}Re - ^{187}Os isochron ages of 77 ± 2 Ma and 80.2 ± 1.3 Ma, respectively, at the Hongshan deposit. The molybdenite separates used are from the quartz-vein-type ores and porphyry-type ores at depth. The predominant skarn-type ore bodies at the Hongshan deposit are not dated, and they are crosscut by the quartz-vein-type ore bodies. The porphyry-type ore bodies are distal to the skarn ore bodies. The timing of the skarn-type Cu-Mo mineralization was thought to be Late Triassic spatially associated with the Triassic dioritic porphyries intrusion (Deng et al., 2012; Hou et al., 2003b; Li et al., 2011a, 2011b; Wang et al., 2008, 2011b; Xu et al., 2006). In this study, the fine-grained (0.02–1 mm) molybdenite separates used for Re-Os dating from the shallow skarn-type Cu mineralization ore body III had high Re contents (19.6 to 80.6 ppm) (Table 3), which implies that the molybdenites might have little or no ^{187}Re decoupling effects thus yielding reliable age data of the molybdenites mineralization (Selby and Creaser, 2004). In addition, disseminated molybdenite in the skarn-type ores coexists with pyrrhotite and chalcopyrite (Fig. 4d–f). These geological features suggest that the molybdenites, pyrrhotite, chalcopyrite, and skarn minerals formed contemporaneously. Therefore, the molybdenite ^{187}Re - ^{187}Os isochron age of 81.2 ± 2.6 Ma (MSWD = 1.3) is

representative of the age of Cu mineralization in the skarn-type ores at Hongshan. Thus, both the skarn-type and porphyry-type mineralization occurred during the Late Cretaceous. This age is similar to the zircon U-Pb age (81.1 ± 0.5 Ma) of the granitic porphyry stocks with weak skarn alteration (Wang et al., 2011b) in the central and the molybdenite ^{187}Re - ^{187}Os isochron age of the porphyry-type molybdenite mineralization (77 ± 2 Ma, Xu et al., 2006; 80.2 ± 1.3 Ma, Li et al., 2011a) in deep areas of the Hongshan deposit. In addition, the Re contents of molybdenites in this region have Re contents varying from 19.7 ppm to 80.6 ppm, which resemble the data (Re = 15–100.1 ppm) reported by Xu et al. (2006) and Li et al. (2011a). This probably indicates a similar and crust–mantle mixed metal source (Mao et al., 1999). These features suggest that shallow skarn-type Cu mineralization is temporally related to the Late Cretaceous granitic porphyry, rather than Triassic intrusions. The $\delta^{34}\text{S}$ values of sulfides (pyrrhotite, chalcopyrite, pyrite, sphalerite, and galena) from the skarn-type ores range from 4.5‰ to 6.2‰, which indicates that the sulfides were formed from a common magma source (Wang et al., 2008). Investigations on fluid inclusions in the quartz veins and comb microfractures within the quartz–chalcopyrite veins from the Hongshan deposit suggest that the Hongshan deposit displays characteristics of the hypogene porphyry copper system (Xu et al., 2006, 2012b). Therefore, the Hongshan deposit is a Late Cretaceous porphyry-skarn Cu-Mo deposit.

6.1.2. Relationship between intrusions and associated ore deposits in the Shangri-La Region

The geological features and zircon U-Pb age data in the Xiuwacu area indicate that the Xiuwacu pluton is a complex massif composed of at least two stages of granitic intrusions: Late Triassic hornblende biotite monzogranite and Late Cretaceous biotite monzogranite (85.6 ± 0.5 Ma and 84.8 ± 0.6 Ma, respectively) and medium-fine grained alkali-feldspar leucogranite (84.4 ± 1.4 Ma). Zircon U-Pb ages of the Late Cretaceous granites in the Xiuwacu deposit are consistent with the Re-Os molybdenite age (83 ± 1 Ma) reported by Li et al. (2007a) within the range of analytical error. Thus, the Mo-W mineralization in the Xiuwacu area is temporally associated with the Late Cretaceous granites rather than the Late Triassic. Zircon U-Pb dating

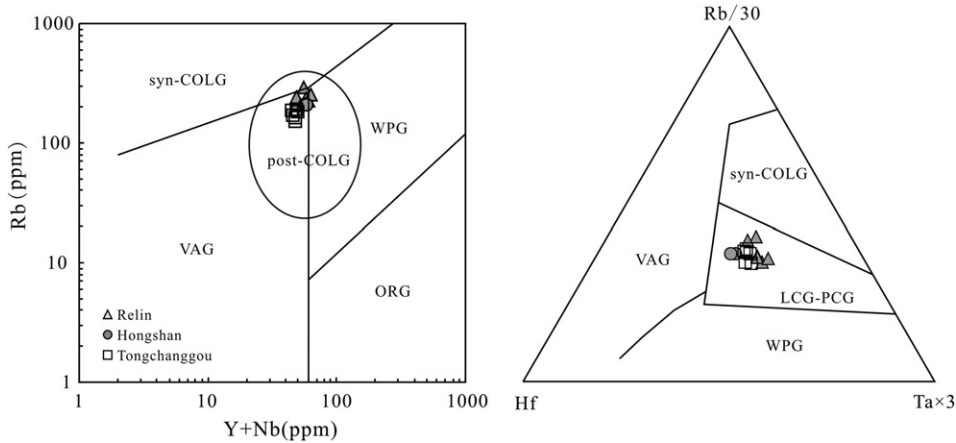


Fig. 13. Rb versus $Y + Nb$ and Rb/30 versus Hf and $Ta \times 3$ discrimination diagrams for the Relin, Hongshan, and Tongchanggou intrusions after Pearce et al. (1984), Pearce (1996), and Harris et al. (1986). Syn-COLG: syn-collisional granites; WPG: within-plate granites; VAG: volcanic arc granites; ORG: oceanic ridge granites; Post-COLG and PCG: post-collisional granites; LCG: late-collisional granites.

results (82.7 ± 0.5 Ma) of the biotite monzogranite in the Relin district are in good agreement with the biotite Ar–Ar ages (81.7–82.0 Ma; Yin et al., 2009) and the Re–Os molybdenite age (81.2 ± 2.3 Ma; Li et al., 2007a) within the range of analytical error. In the Tongchanggou deposit, the biotite monzogranite formed at 87.4–86.3 Ma, which is consistent with the Re–Os molybdenite age of the deposit (85 ± 2 Ma; Li et al., 2012).

Overall, the age results for these four deposits indicate that the magmatism spans from 87.4 ± 0.6 Ma to 76 ± 1.3 Ma and the mineralization processes had a similar time span from 85 ± 2 Ma to 77 ± 2 Ma. In addition, the sulfides from the four deposits were derived from a common magma source (Hou et al., 2003b; Wang et al., 2008). Also, the Re contents of molybdenites from the four deposits are similar, mainly varying from 5.8 to 80.6 ppm. Therefore, the Late Cretaceous Mo–Cu mineralization is spatially, temporally, and probably genetically related to the Cretaceous granites in the Shangri-La region (Fig. 1c).

6.2. Petrogenesis and geodynamic setting

6.2.1. Petrogenesis of the Relin, Hongshan, and Tongchanggou intrusions

As mentioned above, the Xiuwacu pluton is composed of two-stage intrusions. The Xiuwacu Late Cretaceous plutons could have sources similar to the Relin, Hongshan, and Tongchanggou intrusions (Fig. 12),

but with more phases and complicated petrogenesis that will be discussed in another paper in detail.

Rocks from the Relin, Hongshan, and Tongchanggou intrusions have high Sr (363–905 ppm, mostly 400 ppm) and low Y (11.6–17.0 ppm, ≤ 18 ppm) and Yb (0.97–1.41 ppm, ≤ 1.8 ppm), and these data are characteristic of adakitic rocks (Fig. 10; Castillo, 2012; Defant and Drummond, 1990; Martin et al., 2005; Richards and Kerrich, 2007). Generally, adakitic rocks has been proposed to have formed through several mechanisms including: (1) directly derived from the partial melting of downgoing oceanic slabs (Defant and Drummond, 1990; Gutscher et al., 2000; Yogodzinski and Kelemen, 1998); (2) high- or low-pressure fractional crystallization of normal arc basaltic magmas, either with or without assimilation of the crust (Chiardia, 2009; Dessimoz et al., 2012; Macpherson et al., 2006; Richards and Kerrich, 2007); (3) low-pressure fractional crystallization of basaltic magmas (Li et al., 2009); (4) partial melting of the delaminated lower continental crust (Gao et al., 2004; Huang et al., 2008; Kay and Kay, 1993); and (5) partial melting of the thickened lower continental crust (Hou et al., 2004; Wang et al., 2007; Yuan et al., 2010).

The ocean–continent subduction events occurred during the Late Triassic in the Yidun Arc, and then the Yidun Arc collided and accreted with the Songpan-Ganzi Belt in a manner that translated into an intra-continental environment (Hou et al., 2003b; Leng et al., 2012; Wang

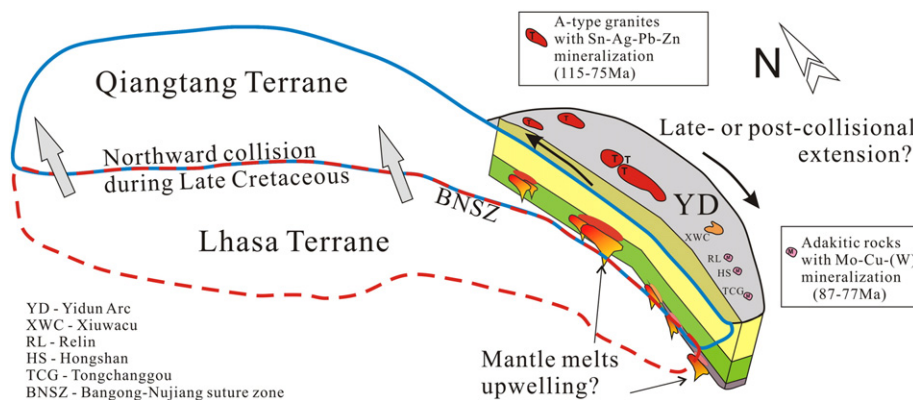


Fig. 14. A suggested model for the generation of Late Cretaceous magmatism and associated Mo–Cu–Ag–Sn–Pb–Zn mineralization in the Yidun Arc. A-type granites with Sn–Ag–Pb–Zn mineralization (115–75 Ma) in the northern Yidun Arc are from Qu et al. (2002). Late Cretaceous granitic intrusions and associated mineralization in the Yidun Arc were generated under late- or post-collision extensional environment related to the northward collision between the Lhasa Terrane and Qiangtang terranes during the Late Cretaceous.

et al., 2011a). Although the Meso- and Neo-Tethys oceanic crust subducted along the Bangong–Nujiang and Yarlung–Zangbo sutures, respectively, there are no other arc-related igneous rocks in the Qiangtang Terrane and Yidun Arc with ages ranging from 105 to 70 Ma. Late Cretaceous arc-related magmas mainly occur in the southern Lhasa Terrane and West Burma Terrane and these have systematically higher $\varepsilon_{\text{Hf}}(\text{t})$ values than those of the Relin, Hongshan, and Tongchanggou intrusions (Fig. 12; Xu et al., 2012c; Zhu et al., 2011a), which indicates that the Relin, Hongshan, and Tongchanggou intrusions could not be generated by partial melting of the downgoing slab or by fractional crystallization of normal arc basaltic magmas. All of these three intrusions had high SiO₂ contents (63–70 wt.%) and negative $\varepsilon_{\text{Hf}}(\text{t})$ values (−7.9 to −2.3), and no contemporaneous basalts have been found in the southern Yidun Arc so far. In addition, there are no positive correlations between SiO₂ and Sr/Y and La/Yb ratios (Figs. 11a and 1b), which indicate that these intrusions could not have formed by high- or low-pressure fractional crystallization of basaltic magmas.

All rocks from the Relin, Hongshan, and Tongchanggou intrusions have negative $\varepsilon_{\text{Hf}}(\text{t})$ values (−7.9 to −2.3, average −5.0) and high K₂O (K₂O/Na₂O > 1.0) suggesting a dominant formation from partial melting of delaminated lower continental crust or thickened lower continental crust. The rocks formed from adakitic magmas by partial melting of the delaminated lower continental crust generally have higher MgO (Mg# > 50), Cr (mostly > 30 ppm), and Ni (mostly > 20 ppm) than those of the above three intrusions (Mg#: 28–46; Cr: 14.4–22.2 ppm; Ni: 6.20–9.74 ppm) as a result of assimilation of upper mantle melts during the ascent process (Figs. 11c and d; Gao et al., 2004; Huang et al., 2008; Lee et al., 2007; Xu et al., 2002). Depletion in HREEs and Y of some adakitic rocks can be generally explained by partial melting of the overthickened lower crust (>50 km, ~15 Kbar) (Hou et al., 2004, 2013). The Relin, Hongshan, and Tongchanggou intrusions have relatively high Yb and Y contents and low Sr/Y and La/Yb ratios compared to those of the Miocene adakitic porphyries in Tibet, which are derived from the overthickened lower crust (>50 km) (Fig. 11; Hou et al., 2004, 2013). Batch melting modeling (Fig. 10) shows that these three intrusions could be probably derived from partial melting of garnet amphibolite with garnet as a residual mineral (>12 Kbar, ~40 km; Wang et al., 2006), indicating that the lower crust in this area was thicker than the normal lower continental crust but not thickened more than 50 km (amphibole eclogite or eclogite facies; Hou et al., 2013). Overall, partial melting of the thickened lower continental crust (~40–50 km) is the preferable mechanism for the generation of adakitic magmas that potentially may have formed the Relin, Hongshan, and Tongchanggou intrusions. In addition, because these intrusions have variable $\varepsilon_{\text{Hf}}(\text{t})$ values with higher values that are displaced to the CHUR reference line (Fig. 12), a mantle component could have been involved in the genesis of these granitic magmas.

6.2.2. Geodynamic setting of Late Cretaceous Mo–Cu–(W) mineralization in the Southern Yidun Arc

Geochronological data for these four Mo–Cu–(W) deposits demonstrate that the ages of these intrusions and deposits (87–77 Ma) fall in the age range of the granites (115–75.3 Ma) of the northern Yidun Arc (Fig. 1b; Table 1; Fan, 2009; Guan, 1999; Hou et al., 2003b; Liao and Yao, 1995; Lin, 2010; Lin et al., 2003; Liu, 2003; Liu et al., 2006; Qu et al., 2001, 2002; Reid et al., 2005a, 2007; Yao and Yang, 1996; Ying et al., 2006; Zhang, 1994; Zou et al., 2008). The granites in the Yidun Arc are considered to have been formed in an intra-continental extensional setting resulting from lithosphere delamination after the collision between the Songpan–Ganzi Belt and Yidun Arc (Hou et al., 2001b, 2003a; Qu et al., 2002). However, intra-plate felsic volcanics and A-type granites have been found in the Yidun Arc and Songpan–Ganzi Belt range in ages from 189 Ma to 182 Ma (Hu et al., 2005; Liu et al., 2007; Qu et al., 2003; Zhang, 1994; Zhao et al., 2007), which indicates

that the intra-plate extension happened in the Yidun Arc during the Early Jurassic.

Abundant Late Cretaceous magmatic rocks occur in the West Yunnan and Burma Terrane, and most of the rocks are suggested to be arc-related magmas formed in response to subduction of the Neo-Tethys (Fig. 1a; Cobbing et al., 1986; Mitchell et al., 2012; Morley, 2012; Schwartz et al., 1995; Xu et al., 2012c). The wide distribution of the Late Cretaceous arc igneous rocks in the Lhasa Terrane are also proposed to have been generated by the northward subduction of the Neo-Tethys oceanic crust (Lin et al., 2012; Zhang et al., 2012; Zhu et al., 2011a, 2013). Is it possible that the Late Cretaceous intrusions in the Yidun Arc were also caused by the subduction of the Neo-Tethys? These Late Cretaceous A-type granites and adakitic rocks in the Yidun Arc are mainly derived from crustal sources and they are distinct from those predominantly mantle source-derived arc magmas in the southern Lhasa Terrane (Fig. 12). Other arc-related intrusions (76–52 Ma) generated by the subduction of the Neo-Tethys in the Burma and West Yunnan are much younger (Fig. 12; Xu et al., 2012c). In addition, Late Cretaceous arc-related intrusions rarely occurred in the east Qiangtang Terrane located between the Yidun Arc and Burma Terrane. Therefore, these Late Cretaceous intrusions in the Yidun Arc could not be caused by the subduction of the Neo-Tethys.

The Bangong Meso-Tethys is the northern portion of the Meso-Tethys and the Bangong–Nujiang suture is between the Qiangtang and Lhasa Terrane (Metcalfe, 2006, 2011). Although the subduction direction of the Bangong Meso-Tethys Ocean remains controversial, there is a general consensus concerning the timing of the Lhasa–Qiangtang collision during the Late Jurassic to Early Cretaceous that is supported by stratigraphy and sedimentology studies along the Bangong suture zone (Guynn et al., 2006; Kapp et al., 2005, 2007). Most studies suggest that the collision between the Lhasa and Qiangtang terranes occurred during the Late Cretaceous. Researchers favoring southward subduction of the Bangong Ocean crust have suggested that the Bangong Meso-Tethys oceanic crust subduction did not cease until the late Early Cretaceous after the slab break off, which was recognized by intensified compositional diversity magmatism at ~113 Ma (Fig. 12; Qu et al., 2012; Sui et al., 2013; Zhu et al., 2009a, 2011a, 2013). However, other researchers supporting northward subduction of the Bangong Meso-Tethys have suggested that the occurrence of the middle Cretaceous arc magmatism in the southern Qiangtang Terrane and 132–108 Ma ophiolites with abundant Middle Cretaceous radiolarians in central Tibet indicates that the Bangong Meso-Tethys Ocean did not finally close until Late Cretaceous (Leloup et al., 2012; Zhang et al., 2012 and references therein). Consequently, the intense indentation between the Lhasa Terrane and Qiangtang Terrane probably took place during the late Early Cretaceous to Late Cretaceous (110–80 Ma).

Given the tectonic effect caused by the Indo-Asian collision (Bi et al., 2000; Hou et al., 2003a; Mo et al., 2007; Pan et al., 2012; Royden et al., 1997; Xu et al., 2012a; Yin and Harrison, 2000), the collision between the Lhasa and Qiangtang terranes also probably resulted in regional uplifting and east-side extension. The area of marine sediments in the Qiangtang Terrane and that of the red bed sediments in the Changdu–Simao Terrane decreased from the Early Jurassic to Late Cretaceous (Morley, 2012; Yin and Harrison, 2000; Zhang et al., 2012 and references therein). Combined with the Ganzi and Daocheng granitoids in the Yidun Arc having apatite fission track ages ranging from 154.9 to 81.6 Ma (Lai et al., 2007; Reid et al., 2005a), this suggests that regional uplifting also occurred in the Yidun Arc from the Middle Jurassic to Late Cretaceous. These data indicate that the Late Mesozoic tectonic evolution of the Yidun Arc could have been affected by the Lhasa–Qiangtang collision. In the Rb versus Y + Nb and Rb/30 versus Hf and Ta × 3 diagrams (Fig. 13), all the rocks from the Relin, Hongshan, and Tongchanggou

intrusions fall within the field of late- or post-collision granites. As mentioned above, the ages of these Late Cretaceous intrusions in the Yidun Arc range from 115 Ma to 75 Ma, consistent with the timing of the intense indentation between the Lhasa and Qiangtang terranes (110–80 Ma) (Zhang et al., 2012; Zhu et al., 2009a, 2011a, 2013). Therefore, these Late Cretaceous granites and associated mineralization in the Yidun Arc probably occurred under a late- or post-collision extensional regime related to the collision between the Lhasa and Qiangtang terranes. In addition, the magmatic products of this period are mainly distributed along the north-south (NS) or NW trending strike-slip faults (Hou et al., 2003b), which indicates that this is probably a strike-slip pull-apart extension; however, further work will be necessary to conclusively demonstrate the extensional mechanisms.

Actually, the southern branch of the Meso-Tethys Ocean was also finally closed during subsequent collisions during the Late Cretaceous with regional uplift and strike-slip extensions (Fig. 1a; Cobbing et al., 1986; Metcalfe, 2011; Mitchell et al., 2012; Morley, 2004, 2012; Searle et al., 2007, 2012; Watkinson et al., 2011). The collisions of the Mawgyi Terrane in Myanmar and the Woyla Terrane in Sumatra are generally considered to have occurred at 120–110 Ma and 100–90 Ma, respectively (Fig. 1a; Morley, 2012). Late Cretaceous (~80 Ma) magmatism and associated Sn polymetallic mineralization were also reported in southeast Asia (Morley, 2012; Schwartz et al., 1995), and these were interpreted to have been formed under the post-Lhasa/Qiangtang collisional regime overprinted by influence of the Neo-Tethyan subduction (Mitchell et al., 2012; Morley, 2012; Schwartz et al., 1995; Watkinson et al., 2011; Xu et al., 2012c).

In summary, we suggest that these Late Cretaceous adakitic rocks and the related Mo–Cu–(W) mineralization in the southern Yidun Arc were probably formed under late- or post-collision extension related to the collision between the Lhasa and Qiangtang terranes during the Late Cretaceous (Fig. 14).

6.3. Comparison with contemporaneous intrusions in the Northern Yidun Arc and implications for metallogenesis

Generally, two polymetallic sub-belts related to the Cretaceous granitic intrusions have been recognized in the Yidun Arc, i.e., the Sn–Ag–Pb–Zn polymetallic sub-belt in the north (Hou et al., 2007) and the Mo–Cu sub-belt in the south. However, the genetic mechanisms generating these two different types of mineralization remain unknown. Here, we attempt to compare the igneous events related to the mineralization in the southern and northern Yidun Arc.

The A-type granites in the northern Yidun Arc have relative higher ϵ_{HF} (−3.9 to 0.0) and ϵ_{Nd} (−8.40 to −4.96) values, which suggests that they could be also predominately derived from partial melting of crustal materials with more addition of mantle materials to their sources. They display variable $(^{87}\text{Sr}/^{86}\text{Sr})_i$ (0.7032 to 0.7220) values that are probably indicative of a mixture of mantle melts and metasediments (Qu et al., 2002). Accordingly, they could have been generated by partial melting of crustal rocks in the middle-lower crust level followed by significant fractional crystallization supported by their relatively high zircon saturation temperature (851–860 °C), their Nb, Ta, and HREE concentrations, and their intensive Ba, Sr, and Eu depletion (Moyen, 2009). In addition, partial melting of such felsic crust with addition of some mantle materials could generate F- and Cl-rich, high temperature reduced magmas, which are favorable for Sn, W, and HFSEs mineralization (Creaser et al., 1991; Dall'Agnol et al., 2012; Hou et al., 2003b; Qu et al., 2002). This is similar to the mechanism that generated magmas in the Nanling region of SE China, which hosts large amounts of W and Sn mineralization (Bi et al., 2008; Li et al., 2007b, 2009; Zhu et al., 2009b).

By contrast, the Relin, Hongshan, and Tongchanggou intrusions in this study have similar ancient two-stages Hf model ages ($T_{\text{DM2}} =$

1.13–1.62 Ga, average 1.42 Ga) with Late Triassic crustal derived rocks in the northern Yidun Arc ($T_{\text{DM2}} = 1.28$ –1.87 Ga, average 1.50 Ga; Fig. 12; Reid et al., 2007; He et al., 2013), which indicates that Mesoproterozoic crustal materials contribute dominantly to their sources. Combined with their high La/Yb and Sr/Y ratios and slightly negative Eu anomalies, they were probably derived from partial melting of the thickened lower continental crust (garnet amphibolite phase) with minor contributions from mantle melts. Many studies have suggested that breaking down of amphibole during partial melting of the thickened lower continental crust would generate hydrous and high $f\text{O}_2$ magmas, which are favorable magmas to form the porphyry Cu–Mo deposit (Bi et al., 2009; Hou et al., 2011; Pirajno, 2009; Richards, 2011); and melting of ancient crustal materials would supply Mo, W, and other metal elements for mineralization (Hou et al., 2011, 2013). The S isotopes of sulfides from these Late Cretaceous deposits in the northern and southern Yidun Arc suggest that these sulfides are of magmatic origin (Hou et al., 2003b; Wang et al., 2008; Ying et al., 2006); these data indicate that the mineralization is genetically related to these intrusive events. Therefore, mixing of mantle- and sediment-derived melts probably generates favorable magmas for Sn-polymetallic mineralization in the northern Yidun Arc; whereas, partial melting of thickened lower continental crust with minor contributions from mantle melts would give rise to fertile magmas for porphyry Mo–Cu mineralization in the southern Yidun Arc (Fig. 1b).

7. Conclusions

- (1) The Hongshan deposit is a porphyry-skarn Cu–Mo deposit. Molybdenite Re–Os ages of skarn-type mineralization in the Hongshan deposit demonstrate that both the skarn-type and porphyry-type mineralization in the Hongshan deposit occurred during the Late Cretaceous at 81.2 ± 2.6 Ma.
- (2) Molybdenite Re–Os and zircon U–Pb dating results suggest that the Xiuwacu, Relin, Hongshan, and Tongchanggou deposits are temporally and probably genetically associated with the Late Cretaceous granitic magmas, and these formed a Mo–Cu belt in the southern Yidun Arc.
- (3) The Relin, Hongshan, and Tongchanggou intrusions have adakitic affinities, and they are probably derived primarily from partial melting of the thickened lower continental crust.
- (4) Based on the timing and petrogenesis of those Late Cretaceous intrusions in the Yidun Arc together with the tectonic evolution of the Meso-Tethys, Late Cretaceous magmatism and mineralization in the southern Yidun Arc formed under a late- or post-collision extensional regime, which was probably related to the collision between the Lhasa and Qiangtang terranes during the Late Cretaceous.

Acknowledgments

This study was jointly supported by “the Key Natural Science Foundation of China (41130423) and the 12th Five-Year Plan Project of the State Key Laboratory of Ore Deposit Geochemistry, Chinese Academy of Sciences (SKLODG-ZY125-03).” We thank Prof. Zhao-Chu Hu, Ms. Xiao-Hong Wang, and Mr. Xiang-Yang Lin for the LA-ICP-MS U–Pb dating; Ms. Liang-Liang Wang and Dr. Sai-Hong Yang for the zircon CL imaging; and Prof. Liang Qi, Ms. Yi-Fan Yin, and Dr. Ying-Ying Liu for the molybdenite Re–Os dating by ICP-MS. Lastly, we are grateful to Dr. Xun Wei, Prof. Zheng-Wei Zhang, and Dr. Jing-Jing Zhu for their useful discussions that generated many ideas, and Prof. Franco Pirajno, Prof. Anthony Reid, and Prof. Di-Cheng Zhu for their constructive and detailed reviews of this manuscript.

Appendix 1. Zircon U-Pb analytical results for each sample

Samples	Pb	U	Th	Th/U	^{207}Pb	$\pm \text{lo}$	^{207}Pb	$\pm \text{lo}$	^{206}pb	$\pm \text{lo}$	^{208}Pb	$\pm \text{lo}$	$^{207}\text{Pb}/^{206}\text{pb}$	$^{207}\text{Pb}/^{235}\text{U}$	$^{206}\text{Pb}/^{238}\text{U}$	$^{208}\text{Pb}/^{232}\text{T}$				
Spot no.	ppm	ppm	ppm		^{206}Pb		^{235}U		^{238}U		^{232}Th		Age (M)	$\pm \text{lo}$	Age (M)	$\pm \text{lo}$	Age (M)	$\pm \text{lo}$		
SXWC10-29																				
1	30.2	714	1954	2.7	0.0473	0.0011	0.0873	0.0022	0.0133	0.0001	0.0043	0.0001	65	54	85	2	85	1	87	2
2	29.4	445	1966	4.4	0.0471	0.0010	0.0875	0.0020	0.0134	0.0001	0.0043	0.0001	54	52	85	2	86	1	87	2
3	18.5	484	1161	2.4	0.0503	0.0017	0.0933	0.0035	0.0133	0.0002	0.0045	0.0001	209	78	91	3	85	1	90	3
4	16.8	337	1099	3.3	0.0489	0.0015	0.0896	0.0027	0.0133	0.0001	0.0041	0.0001	143	69	87	2	85	1	82	2
5	20.9	446	1368	3.1	0.0480	0.0014	0.0886	0.0026	0.0134	0.0001	0.0041	0.0001	98	69	86	2	86	1	84	2
6	23.2	445	1548	3.5	0.0483	0.0012	0.0896	0.0022	0.0134	0.0001	0.0042	0.0001	122	57	87	2	86	1	84	2
7	17.6	461	1121	2.4	0.0466	0.0014	0.0857	0.0026	0.0133	0.0001	0.0041	0.0001	28	70	83	2	85	1	83	2
8	49.1	562	3285	5.8	0.0472	0.0011	0.0886	0.0023	0.0135	0.0001	0.0046	0.0001	61	139	86	2	87	1	92	2
9	13.7	517	821	1.6	0.0483	0.0018	0.0892	0.0033	0.0134	0.0001	0.0043	0.0001	122	89	87	3	86	1	87	2
10	9.45	321	612	1.9	0.0501	0.0021	0.0901	0.0037	0.0131	0.0001	0.0041	0.0001	198	101	88	3	84	1	82	2
11	47.2	885	3123	3.5	0.0490	0.0009	0.0910	0.0018	0.0134	0.0001	0.0044	0.0001	150	43	88	2	86	1	89	2
12	9.21	320	565	1.8	0.0497	0.0020	0.0915	0.0036	0.0134	0.0002	0.0041	0.0001	189	93	89	3	86	1	82	2
13	71.1	1531	4717	3.1	0.0478	0.0009	0.0881	0.0018	0.0133	0.0001	0.0044	0.0001	87	44	86	2	85	1	88	2
14	58.8	611	4139	6.8	0.0473	0.0010	0.0864	0.0022	0.0132	0.0001	0.0044	0.0001	65	56	84	2	84	1	89	2
15	21.5	484	1403	2.9	0.0462	0.0019	0.0854	0.0033	0.0134	0.0002	0.0043	0.0001	6	93	83	3	86	1	86	2
16	31.5	444	2169	4.9	0.0473	0.0012	0.0873	0.0021	0.0134	0.0001	0.0046	0.0001	65	138	85	2	86	1	93	2
17	20.9	389	1399	3.6	0.0501	0.0015	0.0935	0.0030	0.0134	0.0001	0.0045	0.0001	211	72	91	3	86	1	90	3
SXWC10-09																				
1	11.6	527	690	1.3	0.0494	0.0023	0.0894	0.0040	0.0132	0.0002	0.0043	0.0001	169	111	87	4	84	1	87	2
2	27.9	814	1819	2.2	0.0496	0.0015	0.0897	0.0026	0.0131	0.0001	0.0041	0.0001	176	67	87	2	84	1	83	2
3	6.90	300	421	1.4	0.0463	0.0027	0.0858	0.0051	0.0134	0.0002	0.0038	0.0001	9	137	84	5	86	1	77	2
4	30.7	646	2049	3.2	0.0525	0.0016	0.0951	0.0026	0.0132	0.0002	0.0050	0.0003	306	70	92	2	85	1	100	6
5	27.8	833	1781	2.1	0.0508	0.0017	0.0919	0.0028	0.0132	0.0001	0.0046	0.0001	232	76	89	3	84	1	94	2
6	12.8	172	889	5.2	0.0488	0.0018	0.0891	0.0032	0.0132	0.0002	0.0045	0.0002	139	83	87	3	85	1	91	3
7	10.9	190	736	3.9	0.0477	0.0021	0.0881	0.0039	0.0134	0.0002	0.0043	0.0002	83	104	86	4	86	1	86	3
8	24.4	509	1626	3.2	0.0491	0.0015	0.0898	0.0027	0.0132	0.0001	0.0043	0.0002	154	69	87	3	85	1	86	4
9	34.1	979	2197	2.2	0.0463	0.0017	0.0863	0.0036	0.0134	0.0002	0.0042	0.0001	17	85	84	3	86	1	84	2
10	29.9	1576	1757	1.1	0.0479	0.0013	0.0872	0.0027	0.0131	0.0001	0.0042	0.0001	100	67	85	3	84	1	85	2
11	31.2	681	2114	3.1	0.0466	0.0015	0.0861	0.0029	0.0134	0.0002	0.0040	0.0001	33	69	84	3	86	1	81	2
12	28.4	759	1819	2.4	0.0521	0.0020	0.0957	0.0037	0.0133	0.0002	0.0045	0.0001	300	82	93	3	85	1	90	2
13	45.7	715	3235	4.5	0.0521	0.0014	0.0941	0.0027	0.0132	0.0002	0.0047	0.0001	300	58	91	3	84	1	94	2
XWC10-4																				
1	23.0	676	1480	2.2	0.0464	0.0015	0.0844	0.0027	0.0132	0.0001	0.0041	0.0001	20	74	82	3	84	1	83	2
2	86.7	989	6110	6.2	0.0481	0.0007	0.0873	0.0015	0.0131	0.0001	0.0041	0.0001	106	32	85	1	84	1	82	2
3	58.1	636	4185	6.6	0.0506	0.0011	0.0902	0.0021	0.0129	0.0001	0.0046	0.0001	233	50	88	2	82	1	93	3
4	40.6	1396	2618	1.9	0.0491	0.0011	0.0901	0.0022	0.0132	0.0001	0.0041	0.0001	154	56	88	2	85	1	82	2
5	22.1	612	1436	2.3	0.0468	0.0014	0.0852	0.0025	0.0131	0.0001	0.0042	0.0001	39	70	83	2	84	1	84	2
6	79.3	870	5480	6.3	0.0476	0.0009	0.0890	0.0019	0.0135	0.0001	0.0042	0.0001	83	44	87	2	86	1	86	2
RL10-09																				
1	27.2	336	1862	5.5	0.0540	0.0017	0.0968	0.0028	0.0130	0.0002	0.0043	0.0001	372	69	94	3	83	1	86	3
2	49.9	630	3487	5.5	0.0520	0.0014	0.0918	0.0024	0.0128	0.0001	0.0044	0.0001	283	61	89	2	82	1	89	2
3	25.9	415	1762	4.2	0.0513	0.0017	0.0921	0.0029	0.0130	0.0002	0.0041	0.0001	254	69	89	3	83	1	83	2
4	23.1	805	1462	1.8	0.0524	0.0021	0.0930	0.0037	0.0128	0.0001	0.0039	0.0001	302	94	90	3	82	1	80	2
5	14.5	207	1007	4.9	0.0484	0.0019	0.0868	0.0032	0.0130	0.0002	0.0038	0.0001	120	88	85	3	83	1	77	3
6	53.1	576	3732	6.5	0.0534	0.0013	0.0956	0.0025	0.0129	0.0001	0.0050	0.0001	346	90	93	2	83	1	100	3
7	82.9	5754	4390	0.8	0.0540	0.010	0.0962	0.0019	0.0129	0.0001	0.0039	0.0001	369	44	93	2	82	1	80	1
8	51.7	718	3596	5.0	0.0469	0.0011	0.0846	0.0022	0.0130	0.0002	0.0044	0.0001	43	56	82	2	83	1	88	2
9	18.0	616	1149	1.9	0.0515	0.0022	0.0929	0.0045	0.0129	0.0002	0.0038	0.0001	265	103	90	4	83	1	76	2
10	25.2	537	1695	3.2	0.0491	0.0015	0.0888	0.0029	0.0130	0.0002	0.0040	0.0001	154	77	86	3	83	1	81	2
11	37.5	515	2640	5.1	0.0462	0.0014	0.0830	0.0028	0.0129	0.0002	0.0041	0.0001	6	70	81	3	83	1	84	3
12	31.8	513	2197	4.3	0.0480	0.0011	0.0863	0.0020	0.0130	0.0001	0.0041	0.0001	98	47	84	2	83	1	84	2
13	26.5	391	1901	4.9	0.0470	0.0013	0.0835	0.0025	0.0128	0.0001	0.0040	0.0001	56	67	81	2	82	1	80	2
14	48.1	640	3350	5.2	0.0488	0.0011	0.0881	0.0021	0.0131	0.0001	0.0044	0.0001	200	56	86	2	84	1	89	2
15	20.0	355	1443	4.1	0.0506	0.0019	0.0890	0.0036	0.0127	0.0001	0.0039	0.0001	233</td							

Appendix 1 (continued)

Samples	Pb	U	Th	Th/U	^{207}Pb	$\pm \text{lo}$	^{207}Pb	$\pm \text{lo}$	^{206}pb	$\pm \text{lo}$	^{208}Pb	$\pm \text{lo}$	$^{207}\text{Pb}/^{206}\text{Pb}$	$^{207}\text{Pb}/^{235}\text{U}$	$^{206}\text{Pb}/^{238}\text{U}$	$^{208}\text{Pb}/^{232}\text{T}$				
Spot no.	ppm	ppm	ppm		^{206}Pb		^{235}U		^{238}U		^{232}Th		Age (M)	$\pm \text{lo}$	Age (M)	$\pm \text{lo}$	Age (M)	$\pm \text{lo}$		
<i>TCG10-14</i>																				
1	10.8	266	697	2.6	0.0475	0.0014	0.0882	0.0027	0.0135	0.0001	0.0039	0.0001	76	127	86	3	86	1	78	2
2	10.2	219	675	3.1	0.0465	0.0020	0.0865	0.0038	0.0134	0.0002	0.0042	0.0002	33	87	84	4	86	1	85	3
3	12.4	295	807	2.7	0.0497	0.0019	0.0915	0.0034	0.0134	0.0002	0.0040	0.0001	189	117	89	3	86	1	81	3
4	9.85	216	641	3.0	0.0502	0.0024	0.0947	0.0047	0.0137	0.0002	0.0037	0.0002	206	111	92	4	88	1	74	3
5	12.0	299	780	2.6	0.0521	0.0018	0.0967	0.0034	0.0135	0.0001	0.0041	0.0001	300	81	94	3	86	1	83	2
6	11.4	292	740	2.5	0.0485	0.0020	0.0888	0.0035	0.0134	0.0002	0.0040	0.0001	124	94	86	3	86	1	81	2
7	11.2	285	734	2.6	0.0486	0.0017	0.0896	0.0034	0.0133	0.0002	0.0040	0.0001	128	85	87	3	85	1	80	3
8	13.1	302	840	2.8	0.0499	0.0019	0.0932	0.0035	0.0135	0.0001	0.0042	0.0001	191	85	90	3	87	1	85	3
9	10.0	240	641	2.7	0.0473	0.0019	0.0871	0.0034	0.0134	0.0002	0.0040	0.0001	65	102	85	3	86	1	81	3
10	11.9	273	762	2.8	0.0461	0.0021	0.0864	0.0040	0.0136	0.0002	0.0039	0.0001	400	291	84	4	87	1	78	3
11	12.7	342	802	2.3	0.0478	0.0019	0.0896	0.0037	0.0136	0.0002	0.0041	0.0001	87	102	87	3	87	1	82	3
12	11.2	297	715	2.4	0.0458	0.0018	0.0844	0.0031	0.0135	0.0001	0.0040	0.0001	32	84	82	3	86	1	80	2
<i>HS10-03</i>																				
	From Wang et al. (2011b)																			
2	14.3	902	856	1.1	0.0464	0.0019	0.0814	0.0036	0.0127	0.0002	0.0038	0.0001	17	106	79	3	81	1	77	2
3	12.0	356	839	0.4	0.0490	0.0027	0.0847	0.0048	0.0125	0.0002	0.0047	0.0003	146	160	83	5	80	1	96	5
4	15.0	381	1054	0.4	0.0493	0.0020	0.0857	0.0033	0.0126	0.0002	0.0041	0.0001	161	93	84	3	81	1	82	3
5	24.9	620	1712	0.4	0.0466	0.0013	0.0815	0.0022	0.0126	0.0001	0.0039	0.0001	32	63	80	2	81	1	78	2
6	31.0	1655	1780	0.9	0.0507	0.0017	0.0892	0.0028	0.0128	0.0002	0.0042	0.0001	228	76	87	3	82	1	85	2
8	24.8	637	1730	0.4	0.0468	0.0012	0.0815	0.0022	0.0126	0.0001	0.0039	0.0001	39	63	80	2	81	1	79	2
9	21.9	591	1506	0.4	0.0462	0.0012	0.0808	0.0022	0.0126	0.0001	0.0041	0.0001	9	69	79	2	81	1	82	2
10	25.1	1031	1625	0.6	0.0506	0.0016	0.0878	0.0028	0.0125	0.0001	0.0038	0.0001	233	75	85	3	80	1	77	2
11	18.9	478	1292	0.4	0.0567	0.0018	0.0981	0.0031	0.0125	0.0001	0.0043	0.0001	480	70	95	3	80	1	87	3
12	22.7	978	1449	0.7	0.0492	0.0015	0.0866	0.0028	0.0127	0.0001	0.0040	0.0001	167	72	84	3	81	1	80	2
13	11.0	346	740	0.5	0.0495	0.0028	0.0884	0.0061	0.0127	0.0002	0.0043	0.0002	172	133	86	6	81	1	87	5
14	20.6	1319	1168	1.1	0.0547	0.0017	0.0960	0.0031	0.0127	0.0001	0.0039	0.0001	398	75	93	3	81	1	78	1
16	32.8	1186	2158	0.5	0.0485	0.0015	0.0851	0.0027	0.0127	0.0001	0.0038	0.0001	124	69	83	3	82	1	77	2
17	10.5	257	732	0.4	0.0476	0.0025	0.0838	0.0042	0.0128	0.0002	0.0038	0.0002	80	119	82	4	82	1	78	4
19	22.4	491	1570	0.3	0.0517	0.0017	0.0918	0.0033	0.0128	0.0002	0.0043	0.0001	272	74	89	3	82	1	87	3
91500std (44)	17.3	29.0	83.1		0.0749	0.0020	1.8502	0.0510	0.1792	0.0020	0.0540	0.0015	1069	55	1063	18	1062	11	1064	2\
GJ-1 (20)	33.3	8.89	321		0.0601	0.0013	0.8234	0.0185	0.0992	0.0009	0.0322	0.0017	609	47	610	10	610	5	640	3:

Appendix 2. Hf isotope data from zircons of the Relin, Hongshan and Tongchanggou intrusions in the southern Yidun Arc

Spot no.	$^{176}\text{Yb}/^{177}\text{Hf}$	$^{176}\text{Lu}/^{177}\text{Hf}$	$\pm 1\text{a}$	$^{176}\text{Hf}/^{177}\text{Hf}$	$\pm 1\text{a}$	sHf(t)	$\pm 1\text{a}$	$^{\text{tDM1}}$	$^{\text{tDM2}}$	t (Ma)
<i>RL10-09</i>										
1	0.079630	0.001921	0.000059	0.282550	0.000012	-6.1	0.4	1019	1536	82.7
2	0.065080	0.001689	0.000070	0.282524	0.000014	-7.1	0.5	1050	1593	82.7
3	0.095855	0.002324	0.000110	0.282552	0.000018	-6.1	0.6	1028	1532	82.7
4	0.065657	0.001662	0.000049	0.282563	0.000013	-5.7	0.5	993	1506	82.7
5	0.068526	0.001739	0.000038	0.282562	0.000014	-5.7	0.5	997	1508	82.7
6	0.048390	0.001166	0.000036	0.282565	0.000016	-5.6	0.6	977	1500	82.7
7	0.047058	0.001163	0.000017	0.282567	0.000016	-5.5	0.6	975	1495	82.7
8	0.051922	0.001262	0.000050	0.282576	0.000014	-5.2	0.5	964	1475	82.7
9	0.051226	0.001249	0.000027	0.282551	0.000015	-6.1	0.5	999	1531	82.7
10	0.103691	0.002380	0.000096	0.282544	0.000018	-6.4	0.6	1041	1550	82.7
11	0.037986	0.000939	0.000058	0.282564	0.000017	-5.6	0.6	973	1501	82.7
12	0.023691	0.000563	0.000012	0.282580	0.000015	-5.0	0.5	941	1464	82.7
13	0.104168	0.002389	0.000079	0.282608	0.000018	-4.1	0.6	947	1408	82.7
14	0.035046	0.000851	0.000010	0.282546	0.000016	-6.2	0.6	996	1541	82.7
15	0.053501	0.001247	0.000034	0.282547	0.000017	-6.2	0.6	1005	1540	82.7
16	0.053501	0.001247	0.000034	0.282547	0.000017	-6.2	0.6	1005	1540	82.7
17	0.055715	0.001282	0.000035	0.282552	0.000019	-6.0	0.7	999	1529	82.7
18	0.026892	0.000641	0.000035	0.282561	0.000016	-5.7	0.6	970	1507	82.7
19	0.051531	0.001181	0.000025	0.282547	0.000018	-6.2	0.6	1003	1540	82.7
20	0.051524	0.001208	0.000051	0.282555	0.000017	-5.9	0.6	993	1522	82.7
<i>HS10-03</i>										
1	0.028050	0.000737	0.000025	0.282514	0.000014	-7.4	0.5	1038	1613	81.1
2	0.019330	0.000514	0.000041	0.282539	0.000017	-6.5	0.6	997	1556	81.1
3	0.119213	0.002721	0.000180	0.282503	0.000022	-7.9	0.8	1111	1644	81.1
4	0.017114	0.000486	0.000015	0.282554	0.000017	-6.0	0.6	975	1523	81.1
5	0.018636	0.000582	0.000006	0.282556	0.000015	-5.9	0.5	975	1519	81.1
6	0.022035	0.000720	0.000013	0.282526	0.000012	-7.0	0.4	1020	1586	81.1
7	0.027636	0.000738	0.000020	0.282556	0.000011	-5.9	0.4	979	1519	81.1

Appendix 2 (continued)

Spot no.	$^{176}\text{Yb}/^{177}\text{Hf}$	$^{176}\text{Lu}/^{177}\text{Hf}$	$\pm 1\text{a}$	$^{176}\text{Hf}/^{177}\text{Hf}$	$\pm 1\text{a}$	sHf(t)	$\pm 1\text{a}$	T_{DM1}	T_{DM2}	t (Ma)
HS10-03										
8	0.030347	0.000866	0.000014	0.282550	0.000012	-6.1	0.4	991	1533	81.1
9	0.043311	0.001050	0.000039	0.282530	0.000013	-6.8	0.5	1024	1578	81.1
10	0.033543	0.000888	0.000018	0.282558	0.000014	-5.8	0.5	980	1515	81.1
11	0.033445	0.000887	0.000018	0.282552	0.000013	-6.1	0.5	989	1528	81.1
12	0.037394	0.000952	0.000019	0.282550	0.000015	-6.1	0.5	993	1533	81.1
13	0.030483	0.000824	0.000038	0.282540	0.000015	-6.5	0.5	1004	1555	81.1
14	0.087619	0.002025	0.000020	0.282567	0.000016	-5.6	0.6	997	1499	81.1
15	0.051299	0.001176	0.000043	0.282574	0.000013	-5.3	0.5	965	1480	81.1
16	0.035682	0.000942	0.000017	0.282579	0.000014	-5.1	0.5	952	1468	81.1
17	0.031875	0.000842	0.000025	0.282550	0.000015	-6.1	0.5	990	1533	81.1
18	0.021327	0.000559	0.000043	0.282551	0.000016	-6.1	0.6	981	1530	81.1
TCG10-11										
1	0.030012	0.000800	0.000025	0.282602	0.000012	-4.1	0.4	916	1413	87.4
2	0.026894	0.000708	0.000012	0.282655	0.000012	-2.3	0.4	840	1294	87.4
3	0.022336	0.000591	0.000019	0.282614	0.000013	-3.7	0.5	894	1385	87.4
4	0.033983	0.000940	0.000029	0.282610	0.000013	-3.9	0.5	908	1396	87.4
5	0.032183	0.000875	0.000015	0.282608	0.000017	-3.9	0.6	910	1400	87.4
6	0.044668	0.001161	0.000023	0.282614	0.000014	-3.7	0.5	908	1388	87.4
7	0.037637	0.001021	0.000029	0.282617	0.000015	-3.6	0.5	900	1380	87.4
8	0.022487	0.000615	0.000041	0.282616	0.000014	-3.6	0.5	892	1381	87.4
9	0.038017	0.001006	0.000029	0.282582	0.000016	-4.9	0.6	949	1458	87.4
10	0.032359	0.000928	0.000015	0.282606	0.000012	-4.0	0.4	914	1405	87.4
11	0.038516	0.001010	0.000048	0.282636	0.000017	-3.0	0.6	873	1338	87.4
12	0.028479	0.000820	0.000018	0.282623	0.000017	-3.4	0.6	887	1366	87.4
13	0.043609	0.001459	0.000100	0.282592	0.000013	-4.5	0.5	947	1438	87.4
14	0.035420	0.000887	0.000007	0.282594	0.000015	-4.4	0.5	930	1431	87.4
15	0.035615	0.000968	0.000035	0.282582	0.000012	-4.9	0.4	948	1458	87.4
16	0.031838	0.000881	0.000021	0.282597	0.000014	-4.3	0.5	925	1424	87.4
17	0.030209	0.000803	0.000011	0.282625	0.000016	-3.3	0.6	884	1362	87.4
18	0.035190	0.000970	0.000014	0.282635	0.000015	-3.0	0.5	874	1340	87.4
19	0.032363	0.000853	0.000014	0.282602	0.000014	-4.1	0.5	917	1413	87.4

Note: sHf(t) values are calculated using present-day ($^{176}\text{Lu}/^{177}\text{Hf}_{\text{CHUR}} = 0.0332$ and $^{176}\text{Hf}/^{177}\text{Hf}_{\text{CHUR}} = 0.282772$ (Blichert-Toft and Albarède, 1997). T_{DM2} values are calculated using present-day ($^{176}\text{Lu}/^{177}\text{Hf}_{\text{DM}} = 0.0384$ and $^{176}\text{Hf}/^{177}\text{Hf}_{\text{DM}} = 0.28325$ (Griffin et al., 2000). The decay constant of ^{176}Lu is $1.865 \times 10^{-11} \text{ yr}^{-1}$ (Scherer et al., 2001). $^{176}\text{Hf}/^{177}\text{Hf}$ value for the average continental crust is 0.015 (Griffin et al., 2002)

References

- Bi, X.W., Hu, R.Z., Ye, Z.J., Shao, S.X., 2000. Relations between A-type granites and copper mineralization as exemplified by the machangqing Cu deposit. *Sci. China Ser. D Earth Sci.* 43, 93–102.
- Bi, X.W., Li, H.L., Shuang, Y., Hu, X.Y., Hu, R.Z., Peng, J.T., 2008. Geochemical characteristics of fluid inclusions from Qitaoanling A-type granite, Hunan Province, China—Tracing the source of ore forming fluid of the Furong superlarge tin deposit. *Acta Metall. Sin.* 14, 539–548 (in Chinese with English abstract).
- Bi, X.W., Hu, R.Z., Hanley, J., Mungall, J., Peng, J.T., Shang, L.B., Wu, K.X., Suang, Y.A., Li, H.L., Hu, X.Y., 2009. Crystallisation conditions (T, P, fO₂(2)) from mineral chemistry of Cu- and Au-mineralised alkaline intrusions in the Red River-Jinshajiang alkaline igneous belt, western Yunnan Province, China. *Mineral. Petrol.* 96, 43–58.
- Blichert-Toft, J., Albarède, F., 1997. The Lu-Hf isotope geochemistry of chondrites and the evolution of the mantle–crust system. *Earth Planet. Sci. Lett.* 148, 243–258.
- Castillo, P.R., 2012. Adakite petrogenesis. *Lithos* 134, 304–316.
- Castillo, P.R., Janney, P.E., Solidum, R.U., 1999. Petrology and geochemistry of Camiguin Island, southern Philippines: insights to the source of adakites and other lavas in a complex arc setting. *Contrib. Mineral. Petrol.* 134, 33–51.
- Chang, C., 1997. *Geology and Tectonics of Qinghai-Xizang Plateau Solid Earth Sciences Research in China*. Science Press, Beijing (153 pp.).
- Chiaradia, M., 2009. Adakite-like magmas from fractional crystallization and melting-assimilation of mafic lower crust (Eocene Macuchi arc, Western Cordillera, Ecuador). *Chem. Geol.* 265, 468–487.
- Cobbing, E.J., Mallick, D.I.J., Pitfield, P.E.J., Teoh, L.H., 1986. The granites of the Southeast-Asian Tin Belt. *J. Geol. Soc.* 143, 537–550.
- Creaser, R.A., Price, R.C., Wormald, R.J., 1991. A-type granites revisited: assessment of a residual source-model. *Geology* 19, 163–166.
- Dall'Agnol, R., Frost, C.D., Ramo, O.T., 2012. IGC Project 510 “A-type granites and related rocks through time”: Project vita, results, and contribution to granite research. *Lithos* 151, 1–16.
- Defant, M.J., Drummond, M.S., 1990. Derivation of some modern arc magmas by melting of young subducting lithosphere. *Nature* 347, 662–665.
- Deng, J., Hou, Z.Q., Mo, X.X., Yang, L.Q., Wang, Q.F., Wang, C.M., 2010. Superimposed orogenesis and metallogenesis in Sanjiang Tethys. *Mineral Deposits* 29, 37–42 (in Chinese with English abstract).
- Deng, J., Wang, C.M., Li, G.J., 2012. Style and process of the superimposed mineralization in the Sanjiang Tethys. *Acta Petrol. Sin.* 28, 1349–1361.
- Dessimoz, M., Muntener, O., Ulmer, P., 2012. A case for hornblende dominated fractionation of arc magmas: the Chelan Complex (Washington Cascades). *Contrib. Mineral. Petrol.* 163, 567–589.
- Du, A.D., Wu, S.Q., Sun, D.Z., Wang, S.X., Qu, W.J., Markey, R., Stain, H., Morgan, J., Malinovskiy, D., 2004. Preparation and certification of Re-Os dating reference materials: molybdenites HLP and JDC. *Geostand. Geoanal. Res.* 28, 41–52.
- Du, D.D., Qu, X.M., Wang, G.H., Xin, H.B., Liu, Z.B., 2011. Bidirectional subduction of the Middle Tethys oceanic basin in the west segment of Bangonghu-Nujiang suture, Tibet: evidence from zircon U-Pb LA-ICPMS dating and petrogeochemistry of arc granites. *Acta Petrol. Sin.* 27, 1993–2002 (in Chinese with English abstract).
- Fan, X., 2009. Geological features, ore-formation and mineralization zonation of the Hailong-Cuomolong Skarn type Sn-polymetallic deposit in Batang, Sichuan. *Acta Geol. Sichuan* 29, 112–123 (in Chinese with English abstract).
- Gao, S., Ling, W.L., Qiu, Y.M., Lian, Z., Hartmann, G., Simon, K., 1999. Contrasting geochemical and Sm–Nd isotopic compositions of Archean metasediments from the Kongling high-grade terrain of the Yangtze craton: evidence for cratonic evolution and redistribution of REE during crustal anatexis. *Geochim. Cosmochim. Acta* 63, 2071–2088.
- Gao, S., Rudnick, R.L., Yuan, H.L., Liu, X.M., Liu, Y.S., Xu, W.L., Ling, W.L., Ayers, J., Wang, X.C., Wang, Q.H., 2004. Recycling lower continental crust in the North China craton. *Nature* 432, 892–897.
- Griffin, W.L., Pearson, N.J., Belousova, E., Jackson, S.E., van Achterbergh, E., O'Reilly, S.Y., Shee, S.R., 2000. The Hf isotope composition of cratonic mantle: LAM-MC-ICPMS analysis of zircon megacrysts in kimberlites. *Geochim. Cosmochim. Acta* 64, 133–147.
- Griffin, W.L., Wang, X., Jackson, S.E., Pearson, N.J., O'Reilly, S.Y., Xu, X.S., Zhou, X.M., 2002. Zircon chemistry and magma mixing, SE China: in-situ analysis of Hf isotopes, Tonglu and Pingtan igneous complexes. *Lithos* 61, 237–269.
- Guan, S.P., 1999. The petrology of the Rolhorong and Comolong compound granite masses and physicochemical conditions of the formation of associated Sn deposits in western Sichuan. *Tethyan Geol.* 23, 58–72 (in Chinese with English abstract).
- Gutscher, M.A., Maury, R., Eissen, J.P., Bourdon, E., 2000. Can slab melting be caused by flat subduction? *Geology* 28, 535–538.
- Gwynn, J.H., Kapp, P., Pullen, A., Heizer, M., Gehrels, G., Ding, L., 2006. Tibetan basement rocks near Amdo reveal “missing” Mesozoic tectonism along the Bangong suture, central Tibet. *Geology* 34, 505–508.
- Harris, N.B., Pearce, J.A., Tindle, A.G., 1986. Geochemical characteristics of collision-zone magmatism. *Geol. Soc. Lond. Spec. Publ.* 19, 67–81.
- He, D.F., Zhu, W.G., Zhong, H., Ren, T., Bai, Z.J., Fan, H.P., 2013. Zircon U-Pb geochronology and elemental and Sr–Nd–Hf isotopic geochemistry of the Daocheng granitic pluton from the Yidun Arc, SW China. *J. Asian Earth Sci.* 67–68, 1–17.
- Hou, Z.Q., 1993. Tectono-magmatic evolution of the Yidun island-arc and geodynamic setting of Kuroko-type sulfid deposits in Sanjiang region, SW China. *Resour. Geol.* 336–350.
- Hou, Z.Q., Mo, X.X., 1991. A tectono-magmatic evolution of Yidun island arc in Sanjiang region, China. Contribution to the Geology of the Qinghai-Xizang (Tibet) Plateau 153–165 (in Chinese).

- Hou, Z.Q., Zhou, J.R., 2001. Collision-orogenic processes of the Yidun Arc in the Sanjiang Region: record of granites. *Acta Geol. Sin.* 75, 484–497 (in Chinese with English abstract).
- Hou, Z.Q., Khin, Z., Qu, X.M., Ye, Q.T., Yu, J.J., Xu, M.J., Fu, D.M., Yin, X.K., 2001a. Origin of the Gacun volcanic-hosted massive sulfide deposit in Sichuan, China: fluid inclusion and oxygen isotope evidence. *Econ. Geol.* 96, 1491–1512.
- Hou, Z.Q., Qu, X.M., Urabe, T., Takagi, Naito, 2001b. Liquid immiscibility of boninite in Xiangcheng, southwestern China, and its implication to genetic relationship between boninite and komatiitic basalt. *Acta Geol. Sin.-Engl.* 75, 74–93.
- Hou, Z.Q., Ma, H.W., Zaw, K., Zhang, Y.Q., Wang, M.J., Wang, Z., Pan, G.T., Tang, R.L., 2003a. The Himalayan Yulong porphyry copper belt: product of large-scale strike-slip faulting in eastern Tibet. *Econ. Geol.* 98, 125–145.
- Hou, Z.Q., Yang, Y.Q., Wang, H.P., Qu, X.M., Lv, Q.T., Huang, D.H., Wu, X.Z., Yu, J.J., Tang, S.H., Zhao, J.H., 2003b. *Collision-Orogenic Progress and Mineralization System of Yidun Arc*. Geological Publishing House, Beijing (335 pp., in Chinese).
- Hou, Z.Q., Gao, Y.F., Qu, X.M., Rui, Z.Y., Mo, X.X., 2004. Origin of adakitic intrusives generated during mid-Miocene east-west extension in southern Tibet. *Earth Planet. Sci. Lett.* 220, 139–155.
- Hou, Z.Q., Zaw, K., Pan, G.T., Mo, X.X., Xu, Q., Hu, Y.Z., Li, X.Z., 2007. Sanjiang Tethyan metallogenesis in SW China: tectonic setting, metallogenic epochs and deposit types. *Ore Geol. Rev.* 31, 48–87.
- Hou, Z.Q., Zhang, H.R., Pan, X.F., Yang, Z.M., 2011. Porphyry Cu (–Mo–Au) deposits related to melting of thickened mafic lower crust: examples from the eastern Tethyan metallogenic domain. *Ore Geol. Rev.* 39, 21–45.
- Hou, Z.Q., Zheng, Y.C., Yang, Z.M., Rui, Z.Y., Zhao, Z.D., Jiang, S.H., Qu, X.M., Sun, Q.Z., 2013. Contribution of mantle components within juvenile lower-crust to collisional zone porphyry Cu systems in Tibet. *Mineral. Deposita* 48, 173–192.
- Hu, J.M., Meng, Q.R., Shi, Y.R., Qu, H.J., 2005. SHRIMP U–Pb dating of zircons from granitoid bodies in the Songpan–Ganzi terrane and its implications. *Acta Petrol. Sin.* 21, 867–880.
- Hu, Z.C., Gao, S., Liu, Y.S., Hu, S.H., Chen, H.H., Yuan, H.L., 2008. Signal enhancement in laser ablation ICP-MS by addition of nitrogen in the central channel gas. *J. Anal. At. Spectrom.* 23, 1093–1101.
- Huang, F., Li, S.G., Dong, F., He, Y.S., Chen, F.K., 2008. High-Mg adakitic rocks in the Dabie orogen, central China: implications for foundering mechanism of lower continental crust. *Chem. Geol.* 255, 1–13.
- Huang, X.X., Xu, J.F., Chen, J.L., Ren, J.B., 2012. Geochronology, geochemistry and petrogenesis of two periods of intermediate-acid intrusive rocks from Hongshan area in Zhongdian arc. *Acta Petrol. Sin.* 28, 1493–1506.
- Kapp, P., Yin, A., Harrison, T.M., Ding, L., 2005. Cretaceous-Tertiary shortening, basin development, and volcanism in central Tibet. *Geol. Soc. Am. Bull.* 117, 865–878.
- Kapp, P., DeCelles, P.G., Gehrels, G.E., Heizler, M., Ding, L., 2007. Geological records of the Lhasa–Qiangtang and Indo-Asian collisions in the Nima area of central Tibet. *Geol. Soc. Am. Bull.* 119, 917–932.
- Kay, R.W., Kay, S.M., 1993. Delamination and delamination magmatism. *Tectonophysics* 219, 177–189.
- Lai, Q.Z., Ding, L., Wang, H.W., Yue, Y.H., Cai, F.L., 2007. Constraining the stepwise migration of the eastern Tibetan Plateau margin by apatite fission track thermochronology. *Sci. China Ser. D Earth Sci.* 50, 172–183.
- Lee, C.T.A., Morton, D.M., Kistler, R.W., Baird, A.K., 2007. Petrology and tectonics of Phanerozoic continental formation: from island arcs to accretion and continental arc magmatism. *Earth Planet. Sci. Lett.* 263, 370–387.
- Leloup, P.H., Arnaud, N.O., Maheo, G., Paquette, J.L., Guillot, S., Valli, F., Li, H., Xu, Z., Lacassin, R., Tapponnier, P., 2012. Successive deformation episodes along the Lungmu Co zone, west-central Tibet. *Gondwana Res.* 21, 37–52.
- Leng, C.B., Zhang, X.C., Hu, R.Z., Wang, S.X., Zhong, H., Wang, W.Q., Bi, X.W., 2012. Zircon U–Pb and molybdenite Re–Os geochronology and Sr–Nd–Pb–Hf isotopic constraints on the genesis of the Xuejipings porphyry copper deposit in Zhongdian, Northwest Yunnan, China. *J. Asian Earth Sci.* 60, 31–48.
- Li, J.K., Li, W.C., Wang, D.H., Lu, Y.X., Yin, G.H., Xue, S.R., 2007a. Re–Os dating for ore-forming event in the late of Yanshan Epoch and research of ore-forming regularity in Zhongdian Arc. *Acta Petrol. Sin.* 23, 2415–2422.
- Li, X.H., Li, Z.X., Li, W.X., Liu, Y., Yuan, C., Wei, G.J., Qi, C.S., 2007b. U–Pb zircon, geochemical and Sr–Nd–Hf isotopic constraints on age and origin of Jurassic I- and A-type granites from central Guangdong, SE China: major igneous event in response to foundering of a subducted flat-slab? *Lithos* 96, 186–204.
- Li, J.W., Zhao, X.F., Zhou, M.F., Ma, C.Q., de Souza, Z.S., Vasconcelos, P., 2009. Late Mesozoic magmatism from the Daye region, eastern China: U–Pb ages, petrogenesis, and geodynamic implications. *Contrib. Mineral. Petrol.* 157, 383–409.
- Li, W.C., Yin, G.H., Yu, H.J., Lu, Y.X., Liu, X.L., 2011a. The porphyry metallogenesis of Geza volcanic magmatic arc in NW Yunnan. *Acta Petrol. Sin.* 27, 2541–2552.
- Li, W.C., Zeng, P.S., Hou, Z.Q., White, N.C., 2011b. The Pulang porphyry copper deposit and associated felsic intrusions in Yunnan Province, southwest China. *Econ. Geol.* 106, 79–92.
- Li, W.C., Yu, H.J., Yin, G.H., Cao, X.M., Huang, D.Z., Dong, T., 2012. Re–Os dating of molybdenite from Tongchanggou Mo-polymetallic deposit in northwest Yunnan and its metallogenic environment. *Mineral Deposits* 31, 282–292 (in Chinese with English abstract).
- Liao, Y.A., Yao, X.L., 1995. Evolution features and prospecting marks of tiny granite series-unit in Cuomolong, Batang, Sichuan. *J. Mineral. Petrol.* 15, 10–19 (in Chinese with English abstract).
- Lin, Q., 2010. Geological features and prospecting potential for the Xialong Ag–Pb–Zn deposit in Batang, Sichuan. *Acta Geol. Sichuan* 30, 447–461 (in Chinese with English abstract).
- Lin, F.C., Yang, J.R., Chen, C.D., He, X.G., Lin, Q., Lu, Y.X., Liu, Y.C., Xie, E.S., 2003. Potentiability and assessment of Cu–Ag–Pb–Zn–Sn mineral resources in the Yidun metallogenic belt. *Acta Geol. Sichuan* 23, 141–145 (in Chinese with English abstract).
- Lin, I.J., Chung, S.L., Chu, C.H., Lee, H.Y., Gallet, S., Wu, G.Y., Ji, J.Q., Zhang, Y.Q., 2012. Geochemical and Sr–Nd isotopic characteristics of Cretaceous to Paleocene granitoids and volcanic rocks, SE Tibet: petrogenesis and tectonic implications. *J. Asian Earth Sci.* 53, 131–150.
- Liu, Q., 2003. Geological characteristics and genesis of Xiasai silver-polymetallic deposit in western Sichuan Province. *Mineral Deposits* 22, 121–128 (in Chinese with English abstract).
- Liu, X.L., Li, W.C., 2013. The Indo-Chinese magmatism in Gega Arc of Yunnan: evidence from zircon U–Pb dating and Hf isotope composition. *Earth Science Frontiers* (Chinese University of Geosciences–Beijing; Peking University) 20, (in Chinese with English abstract) <http://www.cnki.net/kcms/detail/11.3370.P.20130423.2234.004.html>.
- Liu, S.W., Wang, Z.Q., Yan, Q.R., Li, Q.G., Zhang, D.H., Wang, J.G., 2006. Geochemistry and petrogenesis of Queershuan granitoids, western Sichuan Province. *Acta Geol. Sin.* 80, 1355–1363 (in Chinese with English abstract).
- Liu, Y., Deng, J., Li, C.F., Shi, G.H., Zheng, A.L., 2007. REE composition in scheelite and scheelite Sm–Nd dating for the Xuebaoding W–Sn–Be deposit in Sichuan. *Chin. Sci. Bull.* 52, 2543–2550.
- Liu, Y.S., Hu, Z.C., Gao, S., Gunther, D., Xu, J., Gao, C.G., Chen, H.H., 2008. In situ analysis of major and trace elements of anhydrous minerals by LA-ICP-MS without applying an internal standard. *Chem. Geol.* 257, 34–43.
- Liu, Y.S., Gao, S., Hu, Z.C., Gao, C.G., Zong, K.Q., Wang, D.B., 2010. Continental and oceanic crust recycling-induced melt-peridotite interactions in the Trans-North China Orogen: U–Pb dating, Hf isotopes and trace elements in zircons from mantle xenoliths. *J. Petrol.* 51, 537–571.
- Lu, Y.J., Kerrich, R., McCuaig, T.C., Li, Z.X., Hart, C.J.R., Cawood, P.A., Hou, Z.Q., Bagas, L., Cliff, J., Belousova, E.A., Tang, S.H., 2013. Geochemical, Sr–Nd–Pb, and zircon Hf–O isotopic compositions of Eocene–Oligocene shoshonitic and potassic adakite-like felsic intrusions in western Yunnan, SW China: petrogenesis and tectonic implications. *J. Petrol.* 54, 1309–1348.
- Ludwig, K.R., 2003. *ISOPLOT 3.00: A Geochronological Toolkit for Microsoft Excel*. Berkeley Geochronology Center, Berkeley, California.
- Macpherson, C.G., Dreher, S.T., Thirlwall, M.F., 2006. Adakites without slab melting: high pressure differentiation of island arc magma, Mindanao, the Philippines. *Earth Planet. Sci. Lett.* 243, 581–593.
- Mao, J.W., Zhang, Z.C., Zhang, Z.H., Du, A.D., 1999. Re–Os isotopic dating of molybdenites in the Xiaoliugu (Mo) deposit in the northern Qilian mountains and its geological significance. *Geochim. Cosmochim. Acta* 63, 1815–1818.
- Mao, J.W., Xie, G.Q., Bierlein, F., Qu, W.J., Du, A.D., Ye, H.S., Pirajno, F., Li, H.M., Guo, B.J., Li, Y.F., Yang, Z.Q., 2008. Tectonic implications from Re–Os dating of Mesozoic molybdenum deposits in the East Qinling–Dabie orogenetic belt. *Geochim. Cosmochim. Acta* 72, 4607–4626.
- Martin, H., Smithies, R.H., Rapp, R., Moyen, J.F., Champion, D., 2005. An overview of adakite, tonalite–trondhjemite–granodiorite (TTG), and sanukitoid: relationships and some implications for crustal evolution. *Lithos* 79, 1–24.
- Metcalfe, I., 2006. Paleozoic and Mesozoic tectonic evolution and palaeogeography of East Asian crustal fragments: the Korean Peninsula in context. *Gondwana Res.* 9, 24–46.
- Metcalfe, I., 2011. Tectonic framework and Phanerozoic evolution of Sundaland. *Gondwana Res.* 19, 3–21.
- Metcalfe, I., 2013. Gondwana dispersion and Asian accretion: tectonic and palaeogeographic evolution of eastern Tethys. *J. Asian Earth Sci.* 66, 1–33.
- Middlemost, E.A.K., 1994. Naming materials in the magma/igneous rock system. *Earth Sci. Rev.* 37, 215–224.
- Mitchell, A., Chung, S.L., Oo, T., Lin, T.H., Hung, C.H., 2012. Zircon U–Pb ages in Myanmar: magmatic–metamorphic events and the closure of a neo-Tethys ocean? *J. Asian Earth Sci.* 56, 1–23.
- Mo, X.X., Deng, J.F., Dong, F.L., H, Y.X., Wang, Y., Zhou, S., Yang, W.G., 2001. Volcanic petroetectonic assemblages in Sanjiang Orogenic Belt, SW China and implication for tectonics. *Geol. J. China Univ.* 7, 121–138 (in Chinese with English abstract).
- Mo, X.X., Hou, Z.Q., Niu, Y.L., Dong, G.C., Qu, X.M., Zhao, Z.D., Yang, Z.M., 2007. Mantle contributions to crustal thickening during continental collision: evidence from Cenozoic igneous rocks in southern Tibet. *Lithos* 96, 225–242.
- Morley, C.K., 2004. Nested strike-slip duplexes, and other evidence for Late Cretaceous–Palaeogene transpressional tectonics before and during India–Eurasia collision, in Thailand, Myanmar and Malaysia. *J. Geol. Soc.* 161, 799–812.
- Morley, C.K., 2012. Late Cretaceous–Early Palaeogene tectonic development of SE Asia. *Earth Sci. Rev.* 115, 37–75.
- Moyen, J.F., 2009. High Sr/Y and La/Yb ratios: the meaning of the “adakitic signature”. *Lithos* 112, 556–574.
- Pan, G.T., Xu, Q., Hou, Z.Q., Wang, L.Q., Du, D.X., Mo, X.X., Li, D.M., Wang, M.J., Li, Z.X., Jiang, X.S., Hu, Y.Z., 2003. *Archipelagic Orogenesis Metallogenic Systems and Assessment of the Mineral Resources along the Nujiang–Lanchangjiang–Jinshajiangareain South-Western China*. Geological Publishing House, Beijing (420 pp., in Chinese).
- Pan, G.T., Wang, L.Q., Li, R.S., Yuan, S.H., Ji, W.H., Yin, F.G., Zhang, W.P., Wang, B.D., 2012. *Tectonic evolution of the Qinghai–Tibet Plateau*. *J. Asian Earth Sci.* 53, 3–14.
- Pearce, J., 1996. Sources and settings of granitic rocks. *Episodes* 19, 120–125.
- Pearce, J.A., Harris, N.B.W., Tindle, A.G., 1984. Trace element discrimination diagrams for the tectonic interpretation of granitic rocks. *J. Petrol.* 25, 956–983.
- Peccerillo, A., Taylor, S.R., 1976. Geochemistry of Eocene calc-alkaline volcanic rocks from the Kastamonu area, northern Turkey. *Contrib. Mineral. Petrol.* 58, 63–81.
- Pirajno, F., 2009. *Hydrothermal Processes and Mineral Systems*. Springer, Berlin (1250 pp.).
- Qi, L., Hu, J., Gregoire, D.C., 2000. Determination of trace elements in granites by inductively coupled plasma mass spectrometry. *Talanta* 51, 507–513.
- Qi, L., Zhou, M.F., Wang, C.Y., 2004. Determination of low concentrations of platinum group elements in geological samples by ID-ICP-MS. *J. Anal. At. Spectrom.* 19, 1335–1339.
- Qi, L., Zhou, M.F., Gao, J.F., Zhao, Z., 2010. An improved Carius tube technique for determination of low concentrations of Re and Os in pyrites. *J. Anal. At. Spectrom.* 25, 585–589.

- Qian, Q., Hermann, J., 2013. Partial melting of lower crust at 10–15 kbar: constraints on adakite and TTG formation. *Contrib. Mineral. Petrol.* 165, 1195–1224.
- Qu, X.M., Hou, Z.Q., Zhou, S.G., 2001. Metallogenetic geological characteristics of the Lianlong skarn type Sn–Ag polymetallic deposit in western Sichuan. *Acta Geosci. Sin.* 22, 29–34 (in Chinese with English abstract).
- Qu, X.M., Hou, Z.Q., Zhou, S.G., 2002. Geochemical and Nd, Sr isotopic study of the post-orogenic granites in the Yidun arc belt of northern Sanjiang region, southwestern China. *Resour. Geol.* 52, 163–172.
- Qu, X.M., Hou, Z.Q., Tang, S.H., 2003. Age of intraplate volcanism in the back-arc area of Yidun island arc and its significance. *Petrol. Mineral.* 22, 131–137 (in Chinese with English abstract).
- Qu, X.M., Wang, R.J., Xin, H.B., Jiang, J.H., Chen, H., 2012. Age and petrogenesis of A-type granites in the middle segment of the Bangonghu–Nujiang suture, Tibetan plateau. *Lithos* 146, 264–275.
- Reid, A.J., Fowler, A.P., Phillips, D., Wilson, C.J.L., 2005a. Thermochronology of the Yidun Arc, central eastern Tibetan Plateau: constraints from (40)Ar/(39)Ar K-feldspar and apatite fission track data. *J. Asian Earth Sci.* 25, 915–935.
- Reid, A.J., Wilson, C.J.L., Liu, S., 2005b. Structural evidence for the Permo-Triassic tectonic evolution of the Yidun Arc, eastern Tibetan plateau. *J. Struct. Geol.* 27, 119–137.
- Reid, A.J., Wilson, C.J.L., Shun, L., Pearson, N., Belousova, E., 2007. Mesozoic plutons of the Yidun Arc, SW China: U/Pb geochronology and Hf isotopic signature. *Ore Geol. Rev.* 31, 88–106.
- Richards, J.P., 2011. Magmatic to hydrothermal metal fluxes in convergent and colliding margins. *Ore Geol. Rev.* 40, 1–26.
- Richards, J.R., Kerrich, R., 2007. Special paper: adakite-like rocks: their diverse origins and questionable role in metallogenesis. *Econ. Geol.* 102, 537–576.
- Royden, L.H., Burchfiel, B.C., King, R.W., Wang, E., Chen, Z.L., Shen, F., Liu, Y.P., 1997. Surface deformation and lower crustal flow in eastern Tibet. *Science* 276, 788–790.
- Scherer, E., Münker, C., Mezger, K., 2001. Calibration of the lutetium–hafnium clock. *Science* 293, 683–687.
- Schwartz, M.O., Rajah, S.S., Askury, A.K., Putthapiboon, P., 1995. The southeast Asian tin belt. *Earth Sci. Rev.* 38, 95–286.
- Searle, M.P., Noble, S.R., Cottle, J.M., Waters, D.J., Mitchell, A.H.G., Hlaing, T., Horstwood, M.S.A., 2007. Tectonic evolution of the Mogok metamorphic belt, Burma (Myanmar) constrained by U-Th-Pb dating of metamorphic and magmatic rocks. *Tectonics* 26, TC3014.
- Searle, M.P., Whitehouse, M.J., Robb, L.J., Ghani, A.A., Hutchison, C.S., Sone, M., Ng, S.W.P., Roselee, M.H., Chung, S.L., Oliver, G.J.H., 2012. Tectonic evolution of the Sibumasu–Indochina terrane collision zone in Thailand and Malaysia: constraints from new U-Pb zircon chronology of SE Asian tin granitoids. *J. Geol. Soc.* 169, 489–500.
- Selby, D., Creaser, R.A., 2004. Macroscale NTIMS and microscale LA-MC-ICP-MS Re-Os isotopic analysis of molybdenite: testing spatial restrictions for reliable Re-Os age determinations, and implications for the decoupling of Re and Os within molybdenite. *Geochim. Cosmochim. Acta* 68, 3897–3908.
- Selby, D., Creaser, R.A., Heaman, L.M., Hart, C.J.R., 2003. Re-Os and U-Pb geochronology of the Clear Creek, Dublin Gulch, and Mactung deposits, Tombstone Gold Belt, Yukon, Canada: absolute timing relationships between plutonism and mineralization. *Can. J. Earth Sci.* 40, 1839–1852.
- Shaw, D.M., 1970. Trace element fractionation during anatexis. *Geochim. Cosmochim. Acta* 34, 237–243.
- Shi, D., Zhao, W.J., Brown, L., Nelson, D., Zhao, X., Kind, R., Ni, J., Xiong, J.Y., Mechie, J., Guo, J., Klempner, S., Hearn, T., 2004. Detection of southward intracontinental subduction of Tibetan lithosphere along the Bangong–Nujiang suture by P-to-S converted waves. *Geology* 32, 209–212.
- Smoliar, M.I., Walker, R.J., Morgan, J.W., 1996. Re-Os ages of group IIA, IIIA, IVA, and IVB iron meteorites. *Science* 271, 1099–1102.
- Stein, H.J., Markey, R.J., Morgan, J.W., Du, A., Sun, Y., 1997. Highly precise and accurate Re-Os ages for molybdenite from the East Qinling molybdenum belt, Shaanxi Province, China. *Econ. Geol.* 92, 827–835.
- Stein, H.J., Markey, R.J., Morgan, J.W., Hannah, J.L., Schersten, A., 2001. The remarkable Re-Os chronometer in molybdenite: how and why it works. *Terra Nova* 13, 479–486.
- Sui, Q.L., Wang, Q., Zhu, D.C., Zhao, Z.D., Chen, Y., Santosh, M., Hu, Z.C., Yuan, H.L., Mo, X.X., 2013. Compositional diversity of ca. 110 Ma magmatism in the northern Lhasa Terrane, Tibet: implications for the magmatic origin and crustal growth in a continent–continent collision zone. *Lithos* 168, 144–159.
- Sun, S.S., McDonough, W.F., 1989. Chemical and isotopic systematics of oceanic basalts: implications for mantle composition and processes. *Geol. Soc. Lond. Spec. Publ.* 42, 313–345.
- Suzuki, K., Shimizu, H., Masuda, A., 1996. Re-Os dating of molybdenites from ore deposits in Japan: implication for the closure temperature of the Re-Os system for molybdenite and the cooling history of molybdenum ore deposits. *Geochim. Cosmochim. Acta* 60, 3151–3159.
- Tang, H.F., Zhao, Z.Q., Huang, R.S., Han, Y.J., Su, Y.P., 2008. Primary Hf isotopic study on zircons from the A-type granites in eastern Junggar of Xinjiang, NW China. *Acta Mineral. Sin.* 28, 335–342 (in Chinese with English abstract).
- Wang, X.F., Metcalfe, I., Jian, P., He, L.Q., Wang, C.S., 2000. The Jinshajiang–Ailaoshan Suture Zone, China: tectonostratigraphy, age and evolution. *J. Asian Earth Sci.* 18, 675–690.
- Wang, Q., Xu, J.F., Jian, P., Bao, Z.W., Zhao, Z.H., Li, C.F., Xiong, X.L., Ma, J.L., 2006. Petrogenesis of adakitic porphyries in an extensional tectonic setting, daxing, South China: implications for the genesis of porphyry copper mineralization. *J. Petrol.* 47, 119–144.
- Wang, Q., Wyman, D.A., Xu, J.F., Jian, P., Zhao, Z.H., Li, C.F., Xu, W., Ma, J.L., He, B., 2007. Early Cretaceous adakitic granites in the Northern Dabie Complex, central China: implications for partial melting and delamination of thickened lower crust. *Geochim. Cosmochim. Acta* 71, 2609–2636.
- Wang, S.X., Zhang, X.C., Leng, C.B., Qin, C.J., Wang, W.Q., Zhao, M.X., 2008. Stable isotopic compositions of the Hongshan skarn copper deposit in the Zhongdian area and its implication for the copper mineralization process. *Acta Petrol. Sin.* 24, 480–488.
- Wang, B.Q., Zhou, M.F., Li, J.W., Yan, D.P., 2011a. Late Triassic porphyritic intrusions and associated volcanic rocks from the Shangri-La region, Yidun terrane, Eastern Tibetan Plateau: adakitic magmatism and porphyry copper mineralization. *Lithos* 127, 24–38.
- Wang, X.S., Bi, X.W., Leng, C.B., Tang, Y.Y., Lan, J.B., Qi, Y.Q., Shen, N.P., 2011b. LA-ICP-MS zircon U-Pb dating of granite porphyry in the Hongshan Cu-polymetallic deposit, Zhongdian, northwest Yunnan, China and its Geological Implication. *Acta Mineral. Sin.* 31, 315–321 (in Chinese with English abstract).
- Wang, B.Q., Zhou, M.F., Chen, W.T., Gao, J.F., Yan, D.P., 2013. Petrogenesis and tectonic implications of the Triassic volcanic rocks in the northern Yidun Terrane, Eastern Tibet. *Lithos* 175–176, 285–301.
- Watkinson, I., Elders, C., Batt, G., Jourdan, F., Hall, R., McNaughton, N.J., 2011. The timing of strike-slip shear along the Ranong and Khlong Marui faults, Thailand. *J. Geophys. Res. Solid Earth* 116, B09403.
- Wiedenbeck, M., Alle, P., Corfu, F., Griffin, W.L., Meier, M., Oberli, F., Quadtt, A., Roddick, J.C., Spiegel, W., 1995. Three natural zircon standards for U-Th-Pb, Lu-Hf, trace element and REE analyses. *Geostand. Newslett.* 19, 1–23.
- Woodhead, J., Hergt, J., Shelley, M., Eggins, S., Kemp, R., 2004. Zircon Hf-isotope analysis with an excimer laser, depth profiling, ablation of complex geometries, and concomitant age estimation. *Chem. Geol.* 209, 121–135.
- Xu, J.F., Shinjo, R., Defant, M.J., Wang, Q., Rapp, R.P., 2002. Origin of Mesozoic adakitic intrusive rocks in the Ningzhen area of east China: partial melting of delaminated lower continental crust? *Geology* 30, 1111–1114.
- Xu, X.W., Cai, X.P., Qu, W.J., Song, B.C., Qin, K.Z., Zhang, B.L., 2006. Later Cretaceous granitic porphyritic Cu–Mo mineralization system in the Hongshan area, northwestern Yunnan and its significance for tectonics. *Acta Geol. Sin.* 80, 1422–1433 (in Chinese with English abstract).
- Xu, L.L., Bi, X.W., Hu, R.Z., Zhang, X.C., Su, W.C., Qu, W.J., Hu, Z.C., Tang, Y.Y., 2012a. Relationships between porphyry Cu–Mo mineralization in the Jinshajiang–Red River metallogenic belt and tectonic activity: constraints from zircon U-Pb and molybdenite Re-Os geochronology. *Ore Geol. Rev.* 48, 460–473.
- Xu, X.W., Zhang, B.L., Liang, G.H., Qin, K.Z., 2012b. Zoning of mineralization in hypogene porphyry copper deposits: insight from comb microfractures within quartz–chalcopyrite veins in the Hongshan porphyry Cu deposit, western Yunnan, SW China. *J. Asian Earth Sci.* 56, 218–228.
- Xu, Y.G., Yang, Q.J., Lan, J.B., Luo, Z.Y., Huang, X.L., Shi, Y.R., Xie, L.W., 2012c. Temporal–spatial distribution and tectonic implications of the batholiths in the Gaoligong–Tengliang–Yingjiang area, western Yunnan: constraints from zircon U-Pb ages and Hf isotopes. *J. Asian Earth Sci.* 53, 151–175.
- Yang, Y.Q., Hou, Z.Q., Huang, D.H., Qu, X.M., 2002. Collision orogenic process and magmatic metallogenic system in Zhongdian Arc. *Acta Geosci. Sin.* 23, 17–24 (in Chinese with English abstract).
- Yang, T.N., Hou, Z.Q., Wang, Y., Zhang, H.R., Wang, Z.L., 2012. Late Paleozoic to Early Mesozoic tectonic evolution of northeast Tibet: evidence from the Triassic composite western Jinsha–Garze–Litang suture. *Tectonics* 31, TC4004.
- Yao, X.L., Yang, J., 1996. Determination and Tectonic implication of Gaogong A-type granite in Shiqu. *Acta Geol. Sichuan* 16, 306–314 (in Chinese with English abstract).
- Yin, A., Harrison, T.M., 2000. Geologic evolution of the Himalayan–Tibetan orogen. *Annu. Rev. Earth Planet. Sci.* 28, 211–280.
- Yin, G.H., Li, W.C., Jiang, C.X., Xu, D., Li, J.K., Yang, S.R., 2009. The evolution of Relin uplex rock masses in Yanshan phase and Ar-Ar dating age and copper–molybdenum mineralization characteristics of Zhongdian volcanic–magma arc. *Geol. Explor.* 45, 385–394 (in Chinese with English abstract).
- Ying, H.L., Wang, D.H., Fu, X.F., 2006. Timing and lead and sulfur isotope composition of Xiasai granite and silver polymetallic deposit in Batang, Sichuan Province. *Mineral Deposits* 25, 136–146 (in Chinese with English abstract).
- Yogodzinski, G.M., Kelemen, P.B., 1998. Slab melting in the Aleutians: implications of an ion probe study of clinopyroxene in primitive adakite and basalt. *Earth Planet. Sci. Lett.* 158, 53–65.
- Yuan, C., Zhou, M.F., Sun, M., Zhao, Y.J., Wilde, S., Long, X.P., Yan, D.P., 2010. Triassic granitoids in the eastern Songpan Ganzi Fold Belt, SW China: magmatic response to geodynamics of the deep lithosphere. *Earth Planet. Sci. Lett.* 290, 481–492.
- Yunnan Bureau of Geology and Mineral Resources (YBGM), 1990. Regional Geology of Yunnan Province. Geological Publishing House, Beijing (728 pp., in Chinese).
- Zaw, K., Peters, S.G., Cromie, P., Burrett, C., Hou, Z.Q., 2007. Nature, diversity of deposit types and metallogenic relations of South China. *Ore Geol. Rev.* 31, 3–47.
- Zeng, P.S., Mo, X.X., Yu, Y.H., Hou, Z.Q., Xu, Q.D., Wang, H.P., Li, H., Yang, C.Z., 2003. Porphyries and porphyry copper deposits in Zhongdian area, northwestern Yunnan. *Mineral Deposits* 22, 393–400 (in Chinese with English abstract).
- Zeng, P.S., Wang, H.P., Mo, X.X., Yu, X.H., Li, W.C., Li, T.G., Li, H., Yang, C.Z., 2004. Tectonic setting and prospects of porphyry copper deposits in Zhongdian Island Arc Belt. *Acta Geosci. Sin.* 25, 535–540 (in Chinese with English abstract).
- Zhang, N.D., 1994. Age of granitoids in Baiyu–Dacheng region, west Sichuan. *Acta Geol. Sichuan* 14, 88–99 (in Chinese with English abstract).
- Zhang, K.J., Zhang, Y.X., Tang, X.C., Xia, B., 2012. Late Mesozoic tectonic evolution and growth of the Tibetan plateau prior to the Indo-Asian collision. *Earth Sci. Rev.* 114, 236–249.
- Zhao, Y.J., Yuan, C., Zhou, M.F., Yan, D.P., Long, X.P., Cai, K.D., 2007. Post-orogenic extension of Songpan–Garzê orogen in Early Jurassic: constraints from Niuxingou monzonodiorite and Siguniangshan A-type granite of western Sichuan, China. *Geochemistry* 36, 139–142 (in Chinese with English abstract).
- Zhu, D.C., Mo, X.X., Wang, L.Q., Zhao, Z.D., Niu, Y.L., Zhou, C.Y., Yang, Y.H., 2009a. Petrogenesis of highly fractionated I-type granites in the Zayu area of eastern Gangdese, Tibet: constraints from zircon U-Pb geochronology, geochemistry and Sr-Nd-Hf isotopes. *Sci. China Ser. D Earth Sci.* 52, 1223–1239.
- Zhu, J.C., Wang, R.C., Zhang, P.H., Xie, C.F., Zhang, W.L., Zhao, K.D., Xie, L., Yang, C., Che, X.D., Yu, A.P., Wang, L.B., 2009b. Zircon U-Pb geochronological framework of

- Qitianling granite batholith, middle part of Nanling Range, South China. *Sci. China Ser. D Earth Sci.* 52, 1279–1294.
- Zhu, D.C., Zhao, Z.D., Niu, Y.L., Mo, X.X., Chung, S.L., Hou, Z.Q., Wang, L.Q., Wu, F.Y., 2011a. The Lhasa Terrane: record of a microcontinent and its histories of drift and growth. *Earth Planet. Sci. Lett.* 301, 241–255.
- Zhu, J.L., Hu, R.Z., Bi, X.W., Zhong, H., Chen, H., 2011b. Zircon U–Pb ages, Hf–O isotopes and whole-rock Sr–Nd–Pb isotopic geochemistry of granitoids in the Jinshajiang suture zone, SW China: constraints on petrogenesis and tectonic evolution of the Paleo-Tethys Ocean. *Lithos* 126, 248–264.
- Zhu, D.C., Zhao, Z.D., Niu, Y.L., Dilek, Y., Hou, Z.Q., Mo, X.X., 2013. The origin and pre-Cenozoic evolution of the Tibetan Plateau. *Gondwana Res.* 23, 1429–1454.
- Zou, G.F., Zheng, R.C., Hu, S.H., Chen, C.J., Jiang, H.C., Wu, H.B., 2008. Geological features of the Xiasai silver-polymetallic deposit in West Sichuan, China. *J. Chengdu Univ. Technol. (Sci. Technol. Ed.)* 35, 93–102 (in Chinese with English abstract).